Iron(II) and Cobalt(II) Complexes of *Tris*-Azinyl Analogues of 2,2':6',2''-Terpyridine†,‡

Laurence J. Kershaw Cook[a], Floriana Tuna[b] and Malcolm A. Halcrow*[a]

DOI: 10.1039/c2dt31736b

The syntheses of 2,6-di(pyrid-2-yl)pyrazine (L^1), 2,6-di(pyrazinyl)pyridine (L^2), 2,2':6',2''-terpyrazine (L^3), 2,6-di(pyrimidin-4-yl)pyridine (L^4), 2,6-di(1,2,4-triazin-3-yl)pyridine (L^5), 4-hydroxy-2,6-di(pyrazinyl)pyridine (L^6) and 4-hydroxy-2,6-di(pyrimidin-2-yl)pyridine (L^7) are described. Homoleptic iron(II) and cobalt(II) complexes of these ligands have been prepared and, in four cases, structurally characterised. The iron complexes are all low-spin. However, while the cobalt complexes of the pyrazine-rich ligands L^2, L^3 and L^6 are all predominantly low-spin in the solid state, the other cobalt complexes are essentially high-spin between 5-300 K. The voltammetric M(III)/(II) (M = Fe or Co) oxidations and metal- or ligand-based reductions all become more anodic as the nitrogen content of the ligands increases, which correlates well with Lever's additive electrochemical parameters for the heterocyclic donor groups in each complex.

Introduction

2,2':6',2''-Terpyridine (terpy) and its derivatives form one of the most important ligand classes in transition metal coordination chemistry.[1-5] Complexes of terpy itself can have important functionality, including fluorescence[1,3,6] and spin-crossover.[7] However, terpy derivatives bearing a variety of substituents can also be readily synthesised,[4,8] which has allowed terpy binding sites to be incorporated into many types of molecular and nanochemical device,[3-6,9] supramolecular arrays[2,5,10,11] and metal-containing polymers[4,5,12] and dendrimers.[2,5]

Complexes of other, analogous *tris*-azine derivatives have also proved important, especially in supramolecular chemistry and photochemical devices. The incorporation of additional hydrogen-bond acceptor sites into the terpy skeleton can be a useful approach to constructing hydrogen-bonded host:guest complexes.[10,13] Moreover, nitrogen rich *tris*-azines are better π-acceptors than terpy itself, which can lead to their complexes showing enhanced fluorescence.[14] Finally, derivatives of 2,6-*bis*-(1,2,4-triazinyl)pyridine have proven to be promising candidates for the solvent extraction of actinide elements.[15] Importantly, however, these *tris*-azine ligands and complexes have nearly always been prepared with peripheral substituents, most often at the 4-position of the central pyridyl (or other azinyl) ring.[14-16] That may reflect that common syntheses of *tris*-azines, such as the Kröhnke or Chichibabin reactions, only work well for products that are substituted at the central heterocyclic ring.[4,8]

We describe here the complex chemistry of a series of *tris*-azine terpyridine analogues L^1-L^7 (Scheme 1), concentrating on the parent *tris*-heterocycles lacking any peripheral substituents. Some of these ligands have been synthesised before[17-19] but we are unaware of any previous reports of their coordination

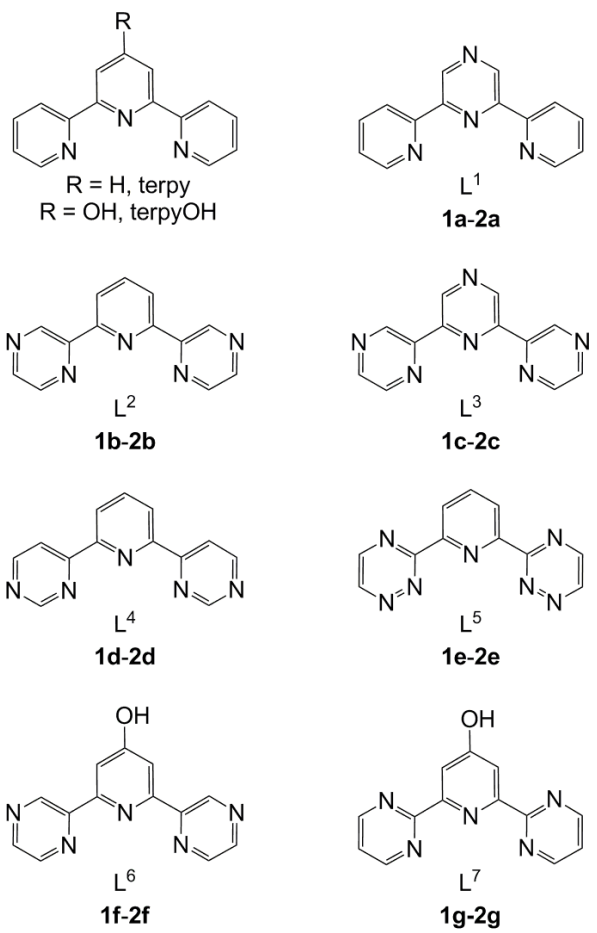

Scheme 1 Ligands used in this work, and the abbreviations used for their iron(II) (**1a**-**1g**) and cobalt(II) (**2a**-**2g**) complexes.

chemistry. Our motivation for this study was two-fold. First, was to investigate the spin- states of their iron and cobalt complexes, as part of our long-standing interest[20,21] in the crystal engineering of spin-crossover materials.[21-23] Salts of $[Co(terpy)_2]^{2+}$ and $[Co(terpyOH)_2]^{2+}$ are a well-established class of spin-crossover compound,[7] while iron(II) complexes of some terpy analogue ligands have also been important in spin-crossover research.[21,24,25] Second, was to find new functional complexes suitable for doping into a spin-crossover lattice, to produce multifunctional switchable materials.[26-29]

Results and Discussion

Ligands L^1-L^5 (Scheme 1) were prepared by variations of literature methods. For L^1-L^3 this involved Stille coupling of 2,6-dibromopyridine or 2,6-dichloropyrazine with the relevant (tributylstannyl)azine precursor.[17] Attempts to prepare 2,6-di(pyrimidin-2-yl)pyridine[30] and 2,6-di(pyrimidin-2-yl)pyrazine by the same Stille coupling route gave only small quantities of impure products, however. Ligands L^4 and L^5 were constructed in two steps from 2,6-diacetylpyridine and 2,6-dicyanopyridine respectively, using standard procedures for the construction of pyrimidine and 1,2,4-triazine rings from those precursor types.[18,19] Notably, we were only able to obtain L^5 in *ca.* 80 % purity by this method,[19] which made it difficult to obtain its complexes in pure form. The new 4-hydroxypyridyl derivatives L^6 and L^7 were obtained by adapting the published procedure for terpyOH (Scheme 1),[31] using pyrazinylcarboxylate and pyrimidin-2-ylcarboxylate esters as starting materials.

The complexes $[FeL_2][BF_4]_2$ (**1a-1g**) and $[CoL_2][BF_4]_2$ (**2a-2g**; Scheme 1) were prepared by treatment of $Fe[BF_4]_2{\cdot}6H_2O$ or $Co[BF_4]_2{\cdot}6H_2O$ with 2 equiv of the relevant ligand. Recrystallisation of the resultant crude materials from $MeNO_2$/Et_2O yielded dark purple (**1a-1g**) and red (**2a-2g**) microcrystalline products in good NMR purity, although several of the compounds retained lattice water or solvent by elemental microanalysis. Unlike the other complexes, pure samples of **1e** and **2e** were only obtained after several recrystallisations, which may reflect their higher solution lability (see below) and the impure nature of the L^5 ligand used. Since pure **1e** and **2e** were only available in mg amounts, they were not characterised to the same extent as the other complexes. The complex salts of terpy and terpyOH were also prepared, for comparison with these new compounds.

Single crystal *X*-ray structures were determined of nitromethane solvates of **1a** and **1d**, and of unsolvated **2b** and **2d**. Interestingly the crystals of **1d** and **2d** are not isostructural, despite having been produced under the same conditions. The expected six-coordinate metal complex centre was observed in each case (Figs. 1 and 2). None of the compounds is isostructural with $[M(terpy)_2][BF_4]_2$ (M^{2+} = Co^{2+}, Cu^{2+} or Ru^{2+}), which all adopt the layered "terpyridine embrace" lattice type[32] in the space group *Cc*.[26,29,33] However, **1a**·$MeNO_2$ and **2b** both adopt different versions of the terpyridine embrace structure, in $P2_1/c$ and $P\bar{4}2_1c$ respectively. The other two structures adopt different crystal packing modes, with no intermolecular π-π interactions between the complex cations. The metric parameters imply that **1a** and **1d** are low-spin at 150 K (Table 1), which is consistent with their susceptibility and NMR data (see below). The Fe–N distances in**1b** are typical of values seen in $[Fe(terpy)_2]^{2+}$ derivatives,[34]

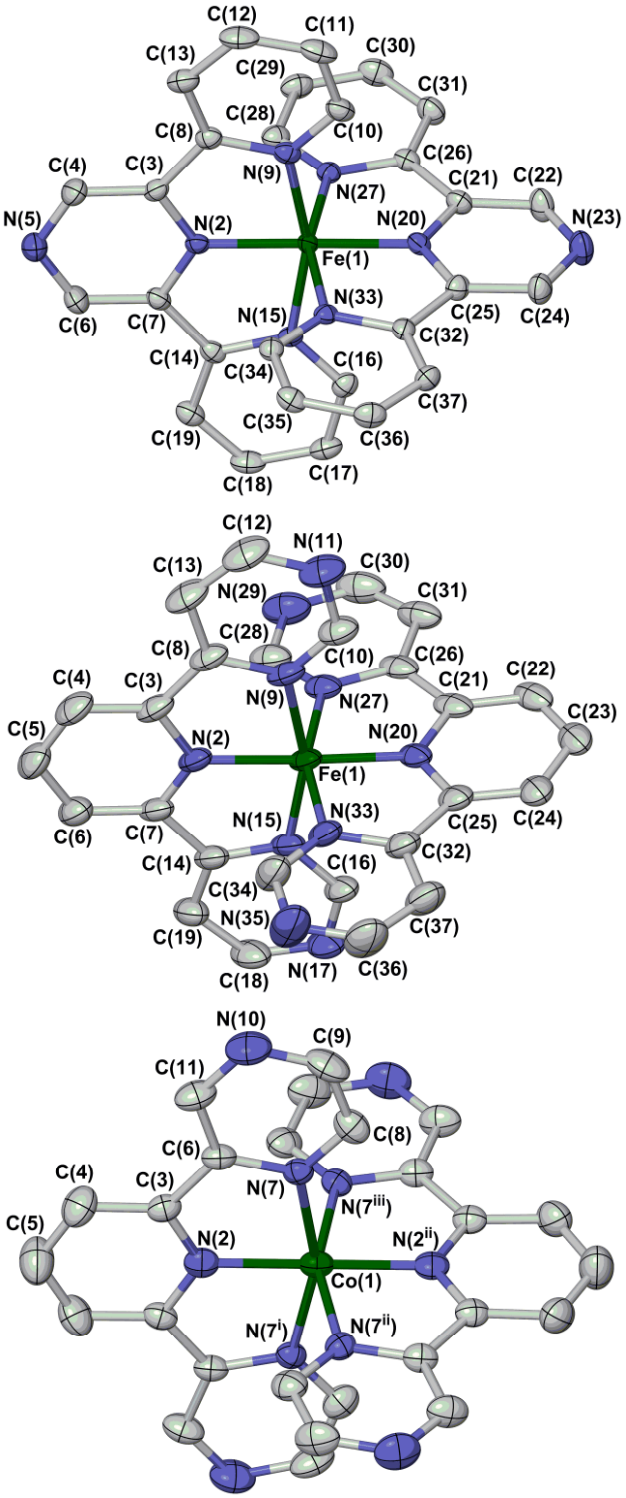

Fig. 1 Views of the $[Fe(L^1)]^{2+}$ cation in **1b**·$MeNO_2$ (top), $[Fe(L^4)]^{2+}$ cation in **1d**·3$MeNO_2$ (center), and the $[Co(L^2)]^{2+}$ cation in **2a** (bottom). All H atoms have been omitted for clarity, and thermal ellipsoids are at the 50% probability level. Symmetry codes: (i) –*x*, –*y*, *z*; (ii) *y*, –*x*, –*z*; (iii) –*y*, *x*, –*z*. Colour code: C, white; Co or Fe, green; N, blue.

but those in **1d** are 0.018(5)-0.041(5) Å longer (Table 1). That may reflect the reduced basicity of the pyrimidinyl N donors in L^4, compared to the distal pyridyl groups in terpy and in L^1.

Table 1 Selected bond distances and angles in the crystal structures of the iron complexes in this work (Å, º). See Fig. 1 for the atom numbering schemes employed, and ref. 21 for a discussion of the distortion indices Σ and Θ which are characteristic for the spin-states of the complexes.

	1a·$MeNO_2$	**1d**·3$MeNO_2$
Fe(1)–N(2)	1.879(4)	1.920(3)
Fe(1)–N(9)	1.998(4)	2.016(2)
Fe(1)–N(15)	1.989(4)	2.013(3)
Fe(1)–N(20)	1.887(4)	1.915(3)
Fe(1)–N(27)	1.998(4)	2.015(3)
Fe(1)–N(33)	1.992(4)	2.023(3)
N(2)–Fe(1)–N(9)	80.57(15)	80.84(11)
N(2)–Fe(1)–N(15)	80.70(15)	80.71(11)
N(2)–Fe(1)–N(20)	179.31(16)	177.87(10)
N(2)–Fe(1)–N(27)	99.86(15)	98.35(11)
N(2)–Fe(1)–N(33)	99.30(15)	100.27(10)
N(9)–Fe(1)–N(15)	161.09(15)	161.55(11)
N(9)–Fe(1)–N(20)	100.12(15)	97.27(11)
N(9)–Fe(1)–N(27)	92.61(14)	92.71(9)
N(9)–Fe(1)–N(33)	90.57(14)	91.06(11)
N(15)–Fe(1)–N(20)	98.60(15)	101.18(10)
N(15)–Fe(1)–N(27)	93.12(14)	89.91(10)
N(15)–Fe(1)–N(33)	89.90(14)	92.25(11)
N(20)–Fe(1)–N(27)	80.15(15)	80.73(11)
N(20)–Fe(1)–N(33)	80.69(15)	80.69(11)
N(27)–Fe(1)–N(33)	160.84(14)	161.36(11)
Σ	82.2(5)	80.2(4)
Θ	264	265

Table 2 Selected bond distances and angles in the crystal structures of the cobalt complexes in this work (Å, º). See Fig. 1 for the atom numbering schemes employed [the numbering for **2d** is the same as for **1d**, but with Fe(1) replaced by Co(1)]. Symmetry codes: (i) *–x, –y, z*; (ii) *y, –x, –z*.

2b		**2d**	
Co(1)–N(2)	1.932(4)	Co(1)–N(2)	2.0659(15)
Co(1)–N(7)	2.099(3)	Co(1)–N(9)	2.1666(15)
		Co(1)–N(15)	2.1482(15)
		Co(1)–N(20)	2.0563(15)
		Co(1)–N(27)	2.1749(16)
		Co(1)–N(33)	2.1928(15)
N(2)–Co(1)–N(7)	79.88(8)	N(2)–Co(1)–N(9)	75.77(6)
		N(2)–Co(1)–N(15)	76.10(6)
N(2)–Co(1)–N(2^{ii})	180	N(2)–Co(1)–N(20)	171.27(5)
N(2)–Co(1)–N(7^{ii})	100.12(8)	N(2)–Co(1)–N(27)	110.33(6)
		N(2)–Co(1)–N(33)	96.43(6)
N(7)–Co(1)–N(7^{i})	159.76(16)	N(9)–Co(1)–N(15)	148.82(6)
		N(9)–Co(1)–N(20)	98.94(6)
N(7)–Co(1)–N(7^{ii})	91.77(3)	N(9)–Co(1)–N(27)	88.88(6)
		N(9)–Co(1)–N(33)	94.83(6)
		N(15)–Co(1)–N(20)	110.52(6)
		N(15)–Co(1)–N(27)	88.45(6)
		N(15)–Co(1)–N(33)	101.42(6)
		N(20)–Co(1)–N(27)	76.15(6)
		N(20)–Co(1)–N(33)	76.91(6)
		N(27)–Co(1)–N(33)	153.05(6)
Σ	88.1(2)	Σ	130.2(2)
Θ	296	Θ	403

The Co–N distances, and the distortion indices Σ and Θ,[21] indicate that **2b** and **2d** are predominantly low-spin and high-spin at 150 K, respectively (Table 2).[33] That is consistent with the magnetic susceptibility data for both compounds, which show they are almost fully low-spin (**2b**) and high-spin (**2d**) at that temperature (see below). The molecular structure of **2d** is notably distorted, with the L^4 ligand N(2)-C(19) being strongly bent; the dihedral angle between the least squares planes of the pyrimidyl rings in this ligand is 19.65(10)º (Fig. 2). A less distorted, but comparable, conformation is also shown by the other ligand in the molecule. This distortion appears to reflect the positioning of an anion in the lattice, which is in van der Waals contact with the pyrimidyl ring C(14)-C(19) and displaces it from coplanarity with its pyridyl substituent. A similar intermolecular van der Waals contact is also present between the other pyrimidyl ring in this ligand C(8)-C(14), and a neighbouring complex molecule (Fig. 2). The distorted molecular structure in **2d** may be responsible for its remaining high-spin at low temperatures (see below), since the suppression of spin-crossover by such conformational distortions has been seen before in iron chemistry.[21,35]

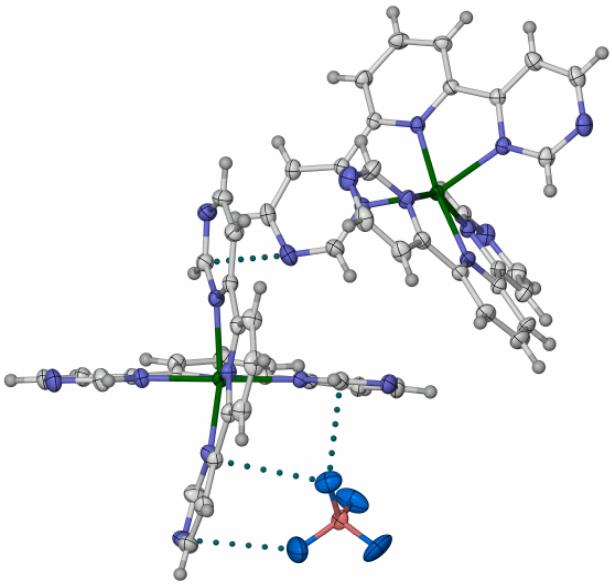

Fig. 2. View of the $[Co(L^4)]^{2+}$ cation in **2d**, emphasising its twisted coordination geometry. Intermolecular steric contacts of 3.0-3.1 Å that may give rise to these structural distortions are also shown. Only one orientation of the disordered BF_4^- ion is included. The atom numbering scheme for this structure is the same as for the $[Fe(L^4)]^{2+}$ cation in Fig. 1, with Fe(1) replaced by Co(1). Colour code: C, white; B, pink; F, cyan; Co, green; N, blue.

X-ray powder diffraction measurements were undertaken on the cobalt complexes (ESI†), to aid interpretion of their magnetic susceptibility data (see below). Solid **2b** has good crystallinity, and is isostructural with the single crystals of that compound. Bulk samples of the other cobalt compounds contain differing proportions of crystalline and amorphous material, with the hydroxylated complexes **2f** and **2g** being predominantly amorphous. Where the peaks were sufficiently resolved, the crystalline components of those samples all appeared to be a single phase; for **2d**, the crystalline fraction is again a good match for the single crystal phase of that complex (ESI†).

All the iron complexes are diamagnetic at room temperature, and yield diamagnetic ^1H NMR spectra in CD_3NO_2 solution. That demonstrates they are low-spin under ambient conditions, in common with most other iron(II) complexes of terpy and its

derivatives.[1,34,36,37] The NMR spectra of the cobalt complexes are paramagnetic, and contain one contact shifted C_2 or *m*-symmetric ligand environment as expected. However, while most of the complexes retain their integrity in solution, **1e** and **2e** are more solution labile on the basis of their ES mass spectra, which predominantly contain peaks from free L^5 and its sodium complex. The ^{1}H NMR spectrum of **2e** also exhibits much smaller contact shifts than for the other cobalt complexes, which may indicate a rapid chemical exchange between free and coordinated L^5.

Solid $[Co(terpy)_2][BF_4]_2$[33] and $[Co(terpyOH)_2][BF_4]_2$[38] both exhibit typically gradual thermal spin-crossover transitions, whose midpoints lie close to room temperature. The spin-state properties of **2a**-**2d**, **2f** and **2g** were therefore investigated through variable temperature magnetic moments (Fig. 3). The behaviour of **2a**, **2d** and **2g** is very similar. All three compounds are predominantly, or fully, high-spin at room temperature and remain so on cooling. The observed decrease in $\chi_M T$ for those compounds at lower temperatures is mostly caused by zero field splitting (ZFS), which is large for high-spin cobalt(II) complexes.[39] Although their lower $\chi_M T$ values imply that a fraction (<20 %) of the cobalt sites in **2a** and **2d** may be undergoing gradual thermal spin-crossover at lower temperatures, that cannot be reliably deconvoluted from ZFS effects in these data. In contrast **2b**, **2c** and **2f** are low-spin at low temperatures, although **2f** retains a residual high-spin fraction of *ca*. 10 %. A gradual increase in $\chi_M T$ for **2b** and **2f** above 200 K and 100 K, respectively, probably reflects the onset of gradual spin-crossover on warming.[7] Unusually, the data for **2f** contain a small anomaly near 265 K, which shows thermal hysteresis when scanned in warming and cooling mode (Fig. 3). The detailed origin of this anomaly could not be elucidated, given the mostly amorphous nature of solid **2f** (ESI†). However, a small number of other cobalt(II) complexes, including $[Co(terpyOH)_2][CF_3SO_3]_2{\cdot}H_2O$, exhibit comparable features in their susceptibility data which are associated with a structural phase transition.[40]

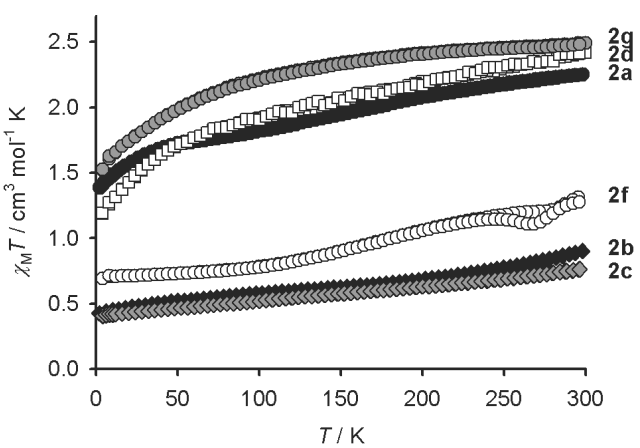

Fig. 3. Variable temperature magnetic susceptibility data for the new cobalt complexes in this work: **2a** (●), **2b** (◆), **2c** (◆), **2d** (□), **2f** (○) and **2g** (●). All the data were obtained using both cooling and warming temperature ramps.

The solid cobalt complexes all show isotropic (g = 2.11-2.12) or axial ($g_{\parallel} \approx 2.23$, $g_{\perp} \approx 2.13$) signals near 120 K by *X*-band EPR spectroscopy, that are typical of $S = {}^1/_2$ $[Co(terpy)_2]^{2+}$-type centres (ESI†).[33,41] Hence **2a**-**2g** all contain a measurable low-spin population at that temperature, although the susceptibility data imply that this should only be a minor fraction of some of the compounds (Fig. 3). The best resolved spectra are for **2d** and **2g**, whose $S = {}^1/_2$ centres are diluted within the predominantly high-spin materials. Warming the samples usually caused significant broadening of these EPR peaks, to the extent that some of the compounds are EPR-silent at room temperature (ESI†). Such strong line-broadening on warming is consistent with partial, or complete, spin-crossover involving these $S = {}^1/_2$ cobalt sites.[33,41] The exceptions to the above generalisation are **2c** and **2d**, whose powder EPR spectra retain their narrow linewidths at room temperature (ESI†). That implies the low-spin fraction of those samples remains low-spin on warming. That is consistent with the susceptibility data for **2c**, which is low-spin between 5-300 K (Fig. 3). For **2d**, this behaviour implies that the low-spin fraction may occupy a separate, minor contaminent phase of that predominantly high-spin material.

Taken together, the susceptibility and EPR data show that solid **2a** and **2g** are predominantly high-spin, but with small fractions of the samples undergoing spin-crossover on cooling; **2d** is essentially high-spin but with a minor low-spin population, possibly in a separate phase of that material; **2c** is low-spin; and, **2b** and **2f** are fully or predominantly low-spin at low-temperature, but show the onset of spin-crossover on warming. Apparent inconsistencies between the susceptibility and EPR data, including the temperature-invariant low-spin content of **2d** and the residual high-spin fraction of **2f** below 100 K, may reflect the presence of both crystalline and amorphous material in those sampels which may show different spin-state properties. In that respect they resemble salts of $[Co(terpy)_2]^{2+}$, whose spin-state behaviour is very sensitive to the presence of solid phases with different degrees of hydration for example.[42]

The UV/vis spectra of the complexes in MeCN are similar in form to those of $[Fe(terpy)_2]^{2+}$ and $[Co(terpy)_2]^{2+}$ derivatives (ESI†).[41,43] All the spectra show the expected MLCT absorptions in the range 450-590 nm. Notably, the MLCT maxima of the hydroxylated complexes are significantly broader than for the other compounds, which probably reflects hydrogen bonding between those complexes and the solvent. Although their extinction coefficients differ somewhat, the MLCT λ_{max} values for $[Fe(terpy)_2][BF_4]_2$, $[Fe(terpyOH)_2][BF_4]_2$ and **1a**-**1c** are almost identical within experimental error, but those of the other iron complexes show more variation. The same is true for the corresponding cobalt compounds. Attempts to explain this trend are complicated, however, because the MLCT envelopes clearly contain at least two distinct absorptions.

Cyclic voltammograms of the complexes in MeCN/0.1 M NBu_4BF_4 at 298 K show more significant variations (Table 3). The M(III)/M(II) couples are fully or partly chemically reversible (except for **2g**, which is irreversible), and fall in the range $+0.54 \leq E_{½} \leq +1.36$ V *vs.* ferrocene/ferrocenium for M = Fe, and $-0.22 \leq E_{½} \leq +0.49$ V for M = Co. All the new compounds **1a**-**1g** and **2a**-**2g** are more difficult to oxidise than the corresponding $[M(terpy)_2]^{2+}$ complex, and the variation in oxidation potential within the iron and cobalt series is broadly similar (ESI†). In particular, the most nitrogen-rich complexes **1c** and **1e**, and **2c** and **2e**, have the highest oxidation potentials; and, hydroxylation

Table 3 Cyclic voltammetry data for the complexes in this work (MeCN/0.1 M NBu_4BF_4, 298 K). Potentials are quoted at a scan rate 100 mV s^{-1}, *vs.* an internal ferrocene/ferrocenium standard. Processes are chemically reversible unless otherwise stated. See the text for the definitions of ΣE_L and ΣpK_a. The data for $[M(terpy)_2][BF_4]_2$, $[M(terpyOH)_2][BF_4]_2$ ($M^{2+} = Fe^{2+}$ and Co^{2+}) closely resemble those reported previously for those compounds.[44-48]

	ΣE_L	ΣpK_a	M(III)/(II) $E_{½}$, V	M(II)/(I) $E_{½}$, V	Ligand-based reductions $E_{½}$, V
$[Fe(terpy)_2][BF_4]_2$	1.50	31.2	+0.71	–	–1.66, –1.81, –1.99
$[Fe(terpyOH)_2][BF_4]_2$	1.42	27.2	+0.54	–	–1.76[b], –1.99, –2.25
1a	1.66	21.6	+0.95	–	–1.30[a], –1.43[a], –2.13, –2.23
1b	1.82	12.0	+1.07[a]	–	–1.25, –1.42, –1.90, –2.16
1c	1.98	2.4	+1.36[a]	–	–0.98, –1.07, –1.73, –1.96[a]
1d	1.66	14.8	+0.98	–	–1.25, –1.41, –1.86, –2.07
1e	–	3.2	+1.20[a]	–	–1.10[b]
1f	1.74	8.0	+0.90[a]	–	–1.09[b]
1g	1.58	10.8	+0.75[a]	–	–1.37[b], –1.59[b]
$[Co(terpy)_2][BF_4]_2$	1.50	31.2	–0.13	–1.17	–2.04
$[Co(terpyOH)_2][BF_4]_2$	1.42	27.2	–0.22	–1.41[b]	–1.95[a]
2a	1.66	21.6	+0.12	–0.81	–1.65, –1.95[a], –2.17[a]
2b	1.82	12.0	+0.22	–0.81[a]	–1.63, –1.90[a], –2.19[a]
2c	1.98	2.4	+0.49	–0.49	–1.32, –1.71, –1.93[a]
2d	1.66	14.8	+0.25	–0.86	–1.59, –1.91, –2.12[a]
2e	–	3.2	+0.18[a]	–0.76[b]	–
2f	1.74	8.0	+0.12[a]	–	–1.11[b], –1.92[b], –2.06[a]
2g	1.58	10.8	+0.17[c]	–	–1.24[b], –1.76[a], –2.11[a]

[a]Partly chemically reversible, $E_{½}$ value quoted. [b]Irreversible process, Ep_c value quoted. [c]Irreversible process, Ep_a value quoted

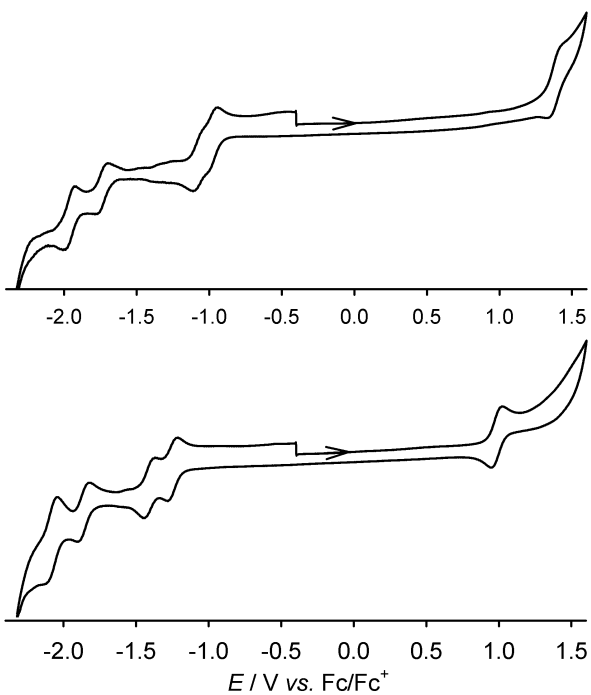

Fig. 4. Representative cyclic voltammograms of two iron complexes in this work, **1c** (top) and **1d** (bottom) (MeCN/0.1 M NBu_4BF_4, 100 mV s^{-1}, 298 K).

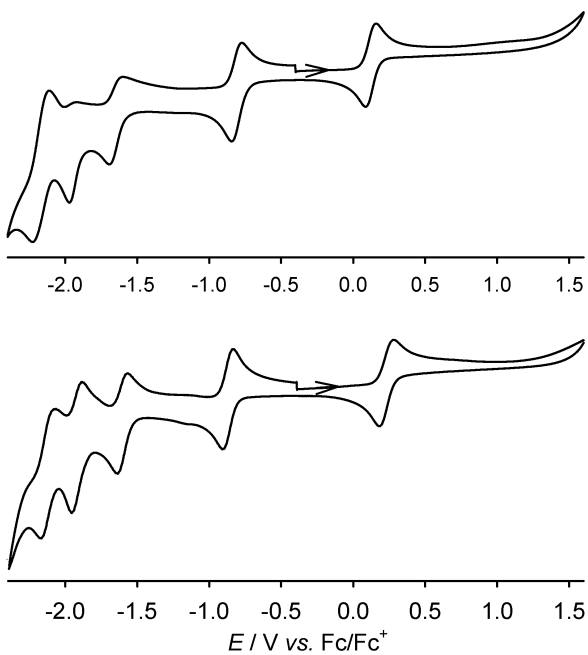

Fig. 5. Representative cyclic voltammograms of two cobalt complexes in this work, **2a** (top) and **2d** (bottom) (MeCN/0.1 M NBu_4BF_4, 100 mV s^{-1}, 298 K).

of the ligands in $[M(terpyOH)_2]^{2+}$ and **2f** makes $E_{½}$ more cathodic compared to their unhydroxylated congeners, by *ca.* 0.15 V for M = Fe and 0.10 V when M = Co.[44,45]

In addition to these oxidations, the complexes show up to four reductive processes within the solvent window (Figs. 4 and 5). These reductions are all fully, or partly, chemically reversible for the complexes of terpy and L^1-L^4. However, the complexes of terpyOH and L^5-L^7 all show an irreversible first reduction. For **1e** and **2e**, that is consistent with the higher lability of those complexes in solution (see above). Otherwise, the data indicate that hydroxylation of the ligand pyridyl donors substantially reduces the kinetic stability of the reduced complexes.

Spectroscopic and theoretical studies have proven that the first two reductions shown by $[Fe(terpy)_2]^{2+}$ are ligand-based, yielding $[Fe(terpy)(terpy^{\bullet-})]^+$ and $[Fe(terpy^{\bullet-})_2]^0$.[46] If the same is true for **1a-1g**, then increasing the nitrogen content in the coordinated ligand heterocycles makes them significantly easier to reduce, by up to 0.6 V based on the first reduction potential. That is consistent with the increased electron deficiency of heterocycles containing multiple heteroatoms.

The first reduction of $[Co(terpy)_2]^{2+}$ is *ca.* 0.5 V more anodic than for its iron analogue (Table 3), and has been ascribed to a cobalt(II)/(I) process.[47,48] The first reductions of $[Co(terpyOH)_2][BF_4]_2$ and **2a-2e** are similarly less negative than for the corresponding iron compounds, and are therefore also assigned to cobalt(II)/(I) processes in the Table although that assignment should be treated as tentative. The second and third reductions for **2a-2d**, presumably $[CoL_2]^+/[Co(L)(L^{\bullet-})]^0$ and $[Co(L)(L^{\bullet-})]^0/[Co(L^{\bullet-})_2]^-$, are also consistently more negative than for the corresponding iron-based ligand reductions by 0.34-0.38 V, and 0.50-0.64 V, respectively (Table 3). That is consistent with the effects of increased back donation from the electron-rich cobalt(I) ion into the ligand π-system. In contrast, the first, irreversible reduction potentials for **2f** and **2g** are much closer to those of **1f** and **1g**, and so are more likely to correspond to ligand-based reductions.

There is a good correlation within the iron and cobalt series between their oxidation potentials and ΣE_L, the sum of Lever's additive E_L electrochemical parameters[49,50] for the parent heterocycles present in the ligands (Table 3 and ESI†). These were calculated using the E_L values for pyridine (0.25), 4-hydroxypyridine (estimated at 0.21, ESI†), pyrimidine (0.29) and pyrazine (0.33).[50] No E_L parameter for 1,2,4-triazine is available, so **1e** and **2e** were not included in the analysis. Reasonable correlations of *E vs.* ΣE_L are also observed for the first reductions shown by both series of complexes,[49] although there is more scatter in those plots than for the oxidation potentials (ESI†).

There is also a weaker relationship between the oxidations and first reductions, and ΣpK_a (Table 3 and ESI†). This is the sum of the basic pK_as of the different ligand donor groups in each molecule: pyridine (pK_a = 5.2), 4-hydroxypyridine (3.2), pyrimidine (1.1), pyrazine (0.4) and 1,2,4-triazine (–1.8).[51] Since M–L π-bonding in divalent first-row transition metal complexes is weak, the electron-richness of the complexes should correlate with the σ-basicity of the coordinated heterocycles. While there is more scatter on the *E vs.* ΣpK_a plots than for the ΣE_L correlations, this is significantly more pronounced for the cobalt reduction waves than for the other processes examined (ESI†). That tentatively supports the above suggestion, that some of the reductions in the cobalt series may be metal centred, and others ligand-centred.

Table 4 The Fe(III)/(II) half-potentials for the different protonation states of the iron/4-hydroxypyridyl complexes in this study (ESI†). Details as for Table 3.

	$[Fe(LOH)_2]^{2+}$	$[Fe(LO^-)(LOH)]^+$	$[Fe(LO^-)_2]^0$
$[Fe(terpyOH)_2][BF_4]_2$	+0.54	+0.38	–0.12
1f	+0.90[a]	–[c]	–[c]
1g	+0.75[a]	+0.48[b]	+0.08[b]

[a]Partly chemically reversible, $E_{½}$ value quoted. [b]Irreversible process, Ep_a value quoted. [c]No peaks observed due to precipitation of the complex.

The voltammograms of the hydroxylated iron complexes were also measured in the presence of 1 or 2 equiv of NBu_4OH, to examine the effects of ligand deprotonation on their oxidation potentials. The results for $[Fe(terpyOH)_2][BF_4]_2$ and **1g** were broadly consistent, in that complete deprotonation of the compounds shifted the iron(III)/(II) couple to more negative potential by 0.66±0.01 V (Table 4, ESI†). Comparable measurements from **1f** were not possible, because the complex precipitated upon addition of base.

Conclusions

The iron(II) and cobalt(II) complexes of L^1-L^7 generally resemble $[Fe(terpy)_2]^{2+}$ and $[Co(terpy)_2]^{2+}$ in their electronic structures, by magnetic susceptibility, UV/vis and (for the cobalt compounds) EPR spectroscopic data. The spin-state behaviour of the cobalt complexes is not always well defined, which may be because the majority of the solid compounds are mixtures of crystalline and amorphous material. However, one observation that can be made is that the pyrazine-rich complexes **2b**, **2c** and **2f** are all predominantly, or fully, low-spin state in the solid state. That is counterintuitive, since the low basic pK_a of a pyrazinyl group implies it should exert a weaker ligand field on a coordinated metal ion (see above). However, it is consistent with previous observations that pyrazine-containing ligands also favour the low-spin state in iron(II) complexes.[52] The pyrimidinyl donors in **2d** and **2f** do not have a comparable effect on the cobalt centre, since those complexes are high-spin.

Increasing the nitrogen content of the ligands generally shifts the metal oxidation, and metal- or ligand-based reduction, potentials of their complexes to more positive values. This is in line with predictions made on the basis of Lever's E_L parameters for the donor groups present in each complex.[49]

The particularly weak dative covalent bonding capability of triazinyl donors in L^5 explains the greater lability of **1e** and **2e** in solution compared to the other complexes. This is evident in their ES mass spectra, in the NMR spectrum of **2e**, and in the poor voltammetric reversibility of their oxidation and reduction processes. It is interesting, however, that the oxidation potentials of **1e** and **2e** are both *ca.* 0.4 V more positive than for analogous complexes of an L^5 derivative bearing ethyl substitutents at the triazine rings.[48] Clearly the electronic structure of the triazine rings in L^5 is very sensitive to substitution.

Previous work has demonstrated that incorporation of diazine or triazine heterocyclic donors into the $[Ru(terpy)_2]^{2+}$ framework significantly enhances its fluorescence lifetime.[14] Preliminary data have shown that the ruthenium(II) complexes of L^1-L^7 also show stronger fluorescent emission than $[Ru(terpy)_2]^{2+}$ in solution at room temperature. We are currently studying this in more detail, and will report these results separately.

Experimental

Unless otherwise stated, all reactions were carried out in air using as-supplied AR-grade solvents. The syntheses of L^1-L^5 followed literature methods,[17-19] but with modified work-ups that led to improved yields or avoided the use of column chromatography. The complexes $[M(terpy)_2][BF_4]_2$ and $[M(terpyOH)_2][BF_4]_2$ (M^{2+} = Fe^{2+} [53] and Co^{2+} [33,38]) were also prepared by the literature methods. Other reagents and solvents were purchased commercially and used as supplied.

Synthesis of 2,6-di(pyrid-2-yl)pyrazine (L^1). 2,6-Dichloropyrazine (1.36 g, 3.69 mmol) and 2-(tributylstannyl)pyridine (0.23 g, 1.54 mmol) were added to a

Schlenk tube containing a 10% catalyst loading of $[Pd(PPh_3)_4]$ (0.32 g) in dry toluene (25 cm^3) under N_2. The black solution was heated to reflux for 48 h, cooled to room temperature and 150 cm^3 of dichloromethane added before filtration. The black filtrate was separated with ammonium hydroxide (100 cm^3) and the organic layer further washed with ammonium hydroxide (3 x 50 cm^3), dried with magnesium sulphate and filtered. The volatiles were removed in vacuo and TLC allowed the collection of the pure product using a silica gel column (eluent: ethyl acetate, R_f value <0.5, streaking at all concentrations tested). Yield 0.14 g, 39 %. ESMS *m/z* 235.1 $[HL^1]^+$. ^{1}H NMR ($CDCl_3$) δ 7.40 (dd, 4.7 and 7.1 Hz, 2H, Py H^5), 7.90 (pseudo-t, 7.7 Hz, 2H, Py H^4), 8.55 (d, 8.1 Hz, 2H, Py H^3), 8.76 (d, 4.4 Hz, 2H, Py H^6), 9.68 (s, 2H, Pyz $H^{3/5}$). ^{13}C NMR ($CDCl_3$) δ 121.5 (2C, Py C^5), 124.4 (2C, Py C^3), 137.0 (2C, Py C^4), 142.8 (2C, Pyz $C^{3/5}$), 149.5 (2C, Py C^6), 149.5 (2C, Pyz $C^{2/6}$), 154.4 (2C, Py C^2).

Synthesis of 2,6-di(pyrazinyl)pyridine (L^2). A Schlenk tube was charged with 2,6-dibromopyridine (0.35 g, 1.48 mmol), 2-(tributylstannyl)pyrazine (1.09 g, 2.96 mmol), $[Pd(PPh_3)_4]$ (0.14 g) and dry toluene (25 cm^3) under N_2 and heated to reflux for 16 h. Water (25 cm^3) was added to the cooled mixture, and the organic layer was extracted with CH_2Cl_2 (3 x 30 cm^3). The resultant solution was dried with magnesium sulphate, filtered and evaporated to dryness. The solid residue was suspended in pentane (50 cm^3) and filtered, yielding the product as a colourless solid. Yield 0.15 g, 42%. Found: C, 65.9; H, 3.80; N, 29.2 %. Calcd for $C_{13}H_9N_5$: C, 66.4; H, 3.86; N, 29.8 %. ESMS *m/z* 236.1 $[HL^2]^+$, 258.1 $[NaL^2]^+$. ^{1}H NMR ($CDCl_3$) δ 8.04 (t, 7.7 Hz, 1H, Py H^4), 8.49 (d, 7.7 Hz, 2H, Py $H^{3/5}$), 8.66 (m, 4H, Pyz H^5 + H^6), 9.85 (d, 0.9 Hz, 2H, Pyz H^3).^{13}C NMR ($CDCl_3$) δ = 122.1 (2C, Py $C^{3/5}$), 138.3 (1C, Py C^4), 143.5, 143.6 and 144.8 (all 2C, Pyz C^3 + C^5 + C^6), 150.8 (2C, Pyz C^2), 153.9 (2C, Py $C^{2/6}$).

Synthesis of 2,2':6',2''-terpyrazine (L^3). A solution of dichloropyrazine (0.18 g, 1.20 mmol) in dry toluene (20 cm^3) was added to a Schlenk tube containing 2-(tributylstannyl)pyrazine (0.96 g, 2.59 mmol) and $[Pd(PPh_3)_4]$ (0.084 g) under N_2 and the reaction mixture left to reflux for 24h. After cooling, 20 cm^3 of water was added to the black solution, and the mixture was extracted with CH_2Cl_2 (3 x 25 cm^3). The solution was dried with $MgSO_4$, which was filtered and washed with 2,2,2-trifluoroethanol (40 cm^3). The combined organic fractions were then evaporated to dryness. The yellow solid was suspended in pentane, filtered and washed with additional pentane and chloroform to leave a colourless solid. Yield 0.14 g, 48 %. Found: C, 56.5; H, 3.15; N, 32.9 %. Calcd for $C_{12}H_8N_6{\cdot}H_2O$: C, 56.7; H, 3.96; N, 33.1 %. ESMS *m/z* 237.1 $[HL^3]^+$, 259.1 $[NaL^3]^+$. ^{1}H NMR ($CDCl_3$) δ 8.04 (t, 7.7 Hz, 1H, Py H^4), 8.49 (d, 7.7 Hz, 2H, Py $H^{3/5}$), 8.66 (m, 4H, Pyz H^5 + H^6), 9.85 (d, 0.9 Hz, 2H, Pyz H^3). ^{1}H NMR ($CDCl_3$) δ 8.70 (s, 4H, distal Pyz H^5 + H^6), 9.66 and 9.76 (both s, 2H, central Pyz $H^{3/5}$ and distal Pyz H^3). The compound was too insoluble for a ^{13}C NMR spectrum to be recorded.

Synthesis of 2,6-di(pyrimidin-4-yl)pyridine (L^4). A solution of 2,6-diacetylpyridine (2.39 g, 14.6 mmol) in *N,N*-dimethylformamide dimethyl acetal (7.0 g, 58.7 mmol) was heated to 120°C for 18 hrs. Concentration of the black mixture to half volume and crystallisation from THF/MeCN yielded 2.40 g (60 %) of 2,6-bis[(*N,N*-dimethylamino)-1-oxoprop-2-en-1-yl]pyridine that was pure by ^{1}H NMR spectroscopy.[##] Formamidine acetate (1.54 g, 14.5 mmol) was added to a flask charged with 2,6-bis[(*N,N*-dimethylamino)-1-oxoprop-2-en-1-yl]pyridine (0.79 g, 2.89 mmol) and boiling ethanol (50 cm^3). A previously prepared solution of sodium (0.70 g, 30.3 mmol) in ethanol (20 cm^3) was then added dropwise over a period of 0.5 h. Reflux was maintained for 16 hrs, after which the dark purple solution was cooled and the ethanol removed *in vacuo*. The residue was dissolved in CH_2Cl_2 and filtered. Column chromatography on neutral alumina (eluent ethyl acetate-hexane, 4:1), followed by recrystallisations from toluene, allowed isolation of the pure product as a colourless solid. Yield 0.27 g, 39 %. Found: C, 63.3; H, 3.65; N, 28.0 %. Calcd for $C_{13}H_9N_5{\cdot}½H_2O$: C, 63.9; H, 4.13; N, 28.7 %. ESMS *m/z* 236.1 $[HL^4]^+$, 258.1 $[NaL^4]^+$. ^{1}H NMR ($CDCl_3$) δ 8.09 (t, 7.8 Hz, 1H, Py H^4), 8.55 (dd, 1.6 and 5.2 Hz, 2H, Pym H^6), 8.66 (d, 7.8 Hz, 2H, Py $H^{3/5}$), 8.95 (d, 5.2 Hz, 2H, Pym H^5), 9.35 (d, 1.2 Hz, 2H, Pym H^2). ^{13}C NMR ($CDCl_3$) δ 117.5 (2C, Pym C^5), 123.4 (2C, Py $C^{3/5}$), 138.6 (1C, Py C^4), 150.3 (2C, Py $C^{2/6}$), 153.7 (2C, Pym C^4), 158.1 and 158.9 (both 2C, 2C, Pym C^2 + C^6).

Synthesis of 2,6-di(1,2,4-triazin-3-yl)pyridine (L^5). Hydrazine monohydrate (5 cm^3) was added to a flask containing 2,6-dicyanopyridine (0.98 g, 7.6 mmol) in ethanol (15 cm^3). The resultant yellow suspension was heated to 55 °C for 4 hrs. After cooling, H_2O was added and the mixture was separated with Et_2O. The resultant precipitate was filtered, washed with Et_2O and dried *in vacuo*. The off-white solid dicarbamidrazone (1.0 g, 5.3 mmol) was then added to a stirring suspension of tri-glyoxal dihydrate (0.73 g, 3.5 mmol) in methanol (50 cm^3) under N_2. The mixture was stirred at room temperature for 3 hrs, then refluxed for a further 2 hrs. After cooling, the suspension was filtered and the bright yellow solid obtained dried *in vacuo*. The product is *ca.* 80 % pure by ^{1}H NMR, but attempts to purify bulk samples by column chromatography or recrystallisation were unsuccessful owing to its poor solubility in useful solvents (mg amounts can be purified by sublimation, with substantial decomposition[19]). ESMS *m/z* 238.1 $[M+H]^+$, 260.1 $[M+Na]^+$, 475.2 $[2M+H]^+$, 497 $[2M+Na]^+$. ^{1}H NMR ($\{CD_3\}_2SO$) δ 8.33 (t, 7.7 Hz, 1H, Py H^4), 8.66 (d, 7.7 Hz, 2H, Py $H^{3/5}$), 9.08 (d, 2.4 Hz, 2H, Tz H^5), 9.55 (d, 2.4 Hz, 2H, Tz H^6). ^{13}C NMR ($\{CD_3\}_2SO$) δ 125.6 (2C, Py $C^{3/5}$), 138.9 (1C, Py C^4), 149.7 and 150.4 (both 2C, Tz C^5 + C^6), 153.2 (2C, Py $C^{2/6}$) 162.7 (2C, Tz C^3).

Synthesis of 2,6-di(pyrazinyl)pyrid-4-one (L^6). To a sodium hydride suspension (60% dispersion in mineral oil, 1.7 g) in 1,2-dimethoxyethane (50 cm^3) under N_2 was added methyl-2-pyrazine carboxylate (3.4 g, 24.6 mmol) and acetone (0.52 g, 9.0 mmol) which caused immediate effervescence. After stirring for 30 mins, the dark red solution was refluxed at 110°C for 6 hrs, cooled to room temperature and the volatiles removed in vacuo. Water (100 cm^3) was added dropwise to the residue yielding a red/orange suspension. Following filtration through celite, the solution was neutralised with dilute hydrochloric acid which afforded a light orange precipitate. The solid 1,5-

di(pyrazinyl)pentane-1,3,5-trione was collected by filtration and dried *in vacuo*. Yield 0.53 g, 22 %. Found: C, 57.0; H, 3.65; N, 19.5 %. Calcd for $C_{13}H_{10}N_4O_3$: C, 57.8; H, 3.73; N, 20.7 %. ESMS *m/z* 271.1 $[M+H]^+$, 293.1 $[M+Na]^+$, 563.2 $[2M+Na]^+$. ^{1}H NMR ($CDCl_3$) δ 6.79 (s, 4H, CH_2), 8.63 (dd, 0.8 and 2.5 Hz, 2H, Pyz H^5), 8.71 (d, 2.5 Hz, 2H, Pyz H^6), 9.28 (d, 0.8 Hz, 2H, Pyz H^3).

1,5-Bis(2'-pyrazinyl)pentane-1,3,5-trione (0.50 g, 1.85 mmol) was added to ammonium acetate (1.14 g, 14.8 mmol) in ethanol (20 cm^3), and the mixture was refluxed for 6 hrs. The dark orange solution was cooled to room temperature and concentrated to half volume. The resultant precipitate was collected, and washed with diethyl ether (20 cm^3) and ethanol (5 cm^3) to yield an off-white solid. Yield 0.41 g, 82 %. Found: C, 60.7; H, 3.55; N, 26.5 %. Calcd for $C_{13}H_9N_5O{\cdot}½H_2O$: C, 60.0; H, 3.87; N, 26.9 %. ESMS *m/z* 252.1 $[HL^6]^+$, 274.1 $[NaL^6]^+$, 503.2 $[H(L^6)_2]^+$, 525.2 $[Na(L^6)_2]^+$. ^{1}H NMR ($\{CD_3\}_2SO$) δ 7.85 (s, 2H, Py $H^{3/5}$), 8.76 (m, 4H, Pyz H^5 & H^6), 9.80 (d, 0.9 Hz, 2H, Pyz H^3), 11.31 (br s, 1H, N*H*). ^{13}C NMR ($\{CD_3\}_2SO$) δ 109.1 (2C, Py $C^{3/5}$), 142.9 (2C, Pyz C^3), 143.9 (2C, Pyz C^5), 145.2 (2C, Pyz C^6), 149.8 (2C, Pyz C^2), 155.1 (2C, Py $C^{2/6}$), 166.2 (1C, Py C^4).

Synthesis of 2,6-di(pyrimid-2-yl)pyrid-4-one (L^7). Under an atmosphere of N_2, a suspension of NaH (60% dispersion in mineral oil, 1.58 g) in glyme (40 cm^3) was stirred for 10 minutes before methyl pyrimidine-2-carboxylate (2.6 g, 19.1 mmol) and acetone (0.46 g, 7.8 mmol) were added, producing a cream coloured suspension. This was stirred for 1 hr h at room temperature, causing a colour change to yellow. The mixture was refluxed at 120°C for 4 h, causing the evolution of H_2 and a gradual darkening to a red-brown colour. After cooling, the volatiles were removed *in vacuo* and H_2O (40 cm^3) carefully added to the solid residue. The resultant orange precipitate was collected, washed with water and dried *in vacuo*. This material was identified as 1,5-di(pyrimid-2-yl)pentane-1,3,5-trione by mass spectrometry, but is too insoluble for its NMR spectra to be recorded. Yield 0.94 g, 44 %. ESMS *m/z* 293.1 $[M + Na]^+$, 563.1 $[2M + Na]^+$.

1,5-Di(pyrimid-2-yl)pentane-1,3,5-trione (0.78 g, 2.9 mmol) and ammonium acetate (2.25 g, 29.2 mmol) were dissolved in dry ethanol (40 cm^3), and refluxed under N_2 for 5 hrs. The cooled solution was concentrated to half its original volume, yielding a yellow solid that was collected by filtration. This was recrystallised from ethanol, and the resultant precipitate triturated in hot acetone to yield a pale yellow powder that was collected and dried. Yield 0.19 g, 27 %. Found: C, 60.7; H, 3.55; N, 26.5 %. Calcd for $C_{13}H_9N_5O{\cdot}½H_2O$: C 60.0; H 3.87; N 26.9 %. ESMS *m/z* 252.1 $[HL^7]^+$, 274.1 $[NaL^7]^+$, 503.2 $[H(L^7)_2]^+$, 525.2 $[Na(L^7)_2]^+$. ^{1}H NMR ($\{CD_3\}_2SO$) δ 7.85 (s, 2H, Py $H^{3/5}$), 8.76 (m, 4H, Pyz H^5 & H^6), 9.80 (d, 0.9 Hz, 2H, Pyz H^3), 11.31 (br s, 1H, N*H*). ^{1}H NMR ($\{CD_3\}_2SO$): 7.37 (br s, 2H, Py $H^{3/5}$), 7.69 (t, 3.3 Hz, 2H, Pym H^5), 9.06 (d, 4.3 Hz, 4H, Pym H^4 + H^6), 11.41 (br s, 1H, N*H*). The compound was too insoluble for a ^{13}C NMR spectrum to be recorded.

Synthesis of the iron(II) and cobalt(II) complexes (1a-1g and 2a-2g). The following method, which describes the synthesis of **1a**, was followed for all these compounds using the appropriate ligand and metal salt. A mixture of $Fe[BF_4]_2{\cdot}6H_2O$ (0.044 g, 13 mmol) and L^1 (0.058 g, 0.25 mmol) in $MeNO_2$ (20 cm^3) was stirred at room temperature, until all the solid had dissolved. The resultant dark purple solution was concentrated *in vacuo* to *ca.* 5 cm^3, and filtered. Slow diffusion of diethyl ether vapor into the filtered solution yielded dark purple microcrystals of **1a**. Yields for the complexes ranged from 70 to 94 %, with all the iron complexes being deep purple solids while the cobalt compounds had a red-orange colouration.

UV/vis and EPR spectroscopy data are given in the ESI†.

For $[Fe(L^1)_2][BF_4]_2$ (**1a**). Found: C, 48.2; H, 2.80; 15.8 %. Calcd. for $C_{28}H_{20}B_2F_8FeN_8$ C, 48.2; H, 2.89; N, 16.1 %. ESMS *m/z* 262.1 $[Fe(L^1)_2]^{2+}$, 611.1 $[Fe(L^1)_2(BF_4)]^+$. ^{1}H NMR (CD_3NO_2) δ 7.16 (t, 4.3 Hz, 4H, H^5), 7.21 (d, 3.8 Hz, 4H, Py H^3), 8.00 (pseudo-t, 5.1 Hz, 4H, Py H^4), 8.72 (d, 6.9 Hz, 4H, Py H^6), 10.14 (s, 4H, Pyz $H^{3/5}$). ^{13}C NMR (CD_3NO_2) δ 126.0 (4C, Py C^5), 129.4 (4C, Py C^3), 140.8 (4C, Py C^4), 144.3 (4C, Pyz $C^{3/5}$), 154.5 (4C, Py C^6), 157.1 and 157.3 (both 4C, Py C^2 and Pyz $C^{2/6}$).

For $[Fe(L^2)_2][BF_4]_2$ (**1b**). Found: C, 44.6; H, 2.55; N, 19.7 %. Calcd. for $C_{26}H_{18}B_2F_8FeN_{10}$: C, 44.5; H, 2.59; N, 20.0 %. ESMS *m/z* 263.1 $[Fe(L^2)_2]^{2+}$, 526.1 $[Fe(L^2)_2]^+$, 545.1 $[Fe(L^2)_2F]^+$. ^{1}H NMR (CD_3NO_2) δ 7.35 (dd, 0.9 and 3.2 Hz, 4H, Pyz H^5), 8.26 (d, 3.2 Hz, 4H, Pyz H^6), 8.86 (t, 8.1 Hz, 2H, Py H^4), 9.12 (d, 8.1 Hz, 4H, Py $H^{3/5}$), 9.61 (d, 0.9 Hz, 4H, Pyz H^3). ^{13}C NMR (CD_3NO_2) δ 126.3 (4C, Py $C^{3/5}$), 141.2 (2C, Py C^4), 145.2 (4C, Pyz C^5), 149.1 (4C, Pyz C^3), 149.7 (4C, Pyz C^6), 154.7 (4C, Py $C^{2/6}$), 160.1 (4C, Pyz C^2).

For $[Fe(L^3)_2][BF_4]_2{\cdot}2H_2O$ (**1c**). Found: C, 38.8; H, 2.55; N, 22.2 %. Calcd. for $C_{24}H_{16}B_2F_8FeN_{12}{\cdot}2H_2O$ C, 39.1; H, 2.73; N, 22.8 %. ESMS *m/z* 264.0 $[Fe(L^3)_2]^{2+}$, 311.0 $[Fe(L^3)F]^+$, 528.1 $[Fe(L^3)_2]^+$, 547.1 $[Fe(L^3)_2F]^+$. ^{1}H NMR (CD_3NO_2) δ 7.36 (dd, 1.1 and 3.2, Hz, 4H, distal Pyz H^5), 8.30 (d, 3.2 Hz, 4H, distal Pyz H^6), 9.78 (d, 1.1 Hz, 4H, distal Pyz H^3), 10.27 (s, 4H, central Pyz $H^{3/5}$). ^{13}C NMR (CD_3NO_2) δ 145.6 (central Pyz $C^{3/5}$), 146.1 (distal Pyz C^5), 149.9 and 150.1 (both 4C, distal Pyz C^3 + C^6), 152.8 and 155.6 (both 4C, central Pyz $C^{2/6}$ and distal Pyz C^2).

For $[Fe(L^4)_2][BF_4]_2{\cdot}H_2O$ (**1d**). Found: C, 43.4; H, 2.70; N, 18.7 %. Calcd. for $C_{26}H_{18}B_2F_8FeN_{10}{\cdot}H_2O$: C, 43.5; H, 2.81; N, 19.5 %. ESMS *m/z* 263.1 $[Fe(L^4)_2]^{2+}$. ^{1}H NMR (CD_3NO_2) δ 7.77 (d, 1.3 Hz, 4H, Pym H^2), 8.52 (dd, 1.3 and 5.1 Hz, 4H, Pym H^5), 8.85 (d, 5.1 Hz, 4H, Pym H^6), 8.94 (t, 8.1 Hz, 2H, Py H^4), 9.29 (d, 8.1 Hz, 4H, Py $H^{3/5}$). ^{13}C NMR ($MeNO_2$-d_3) δ 120.5 (4C, Pym C^5), 129.1 (4C, Py $C^{3/5}$), 140.9 (2C, Py C^4), 154.7 (4C, Py $C^{2/6}$), 161.5 and 162.8 (both 4C, Pym C^2 + C^6), 166.0 (4C, Pym C^4).

For $[Fe(L^5)_2][BF_4]_2{\cdot}2H_2O$ (**1e**). Found: C, 36.0; H, 2.40; N, 25.8 %. Calcd. for $C_{22}H_{14}B_2F_8FeN_{14}{\cdot}2H_2O$: C, 35.7; H, 2.45; N, 26.5 %. ESMS *m/z* 238.1 $[HL^5]^+$, 260.1 $[NaL^5]^+$, 265.0 $[Fe(L^5)_2]^{2+}$, 497 $[Na(L^5)_2]^+$, 617.1 $[Fe(L^5)_2(BF_4)]^+$. ^{1}H NMR (CD_3NO_2) δ 8.87 (t, 7.6 Hz, 4H, Py H^4), 8.89 and 8.93 (both d, 2.1 Hz, 4H, Tz H^5 + H^6), 9.13 (d, 7.6 Hz, 4H, Pyz $H^{3/5}$). ^{13}C NMR ($MeNO_2$-d_3) δ 128.2 (4C, Py $C^{3/5}$), 140.6 (2C, Py C^4), 150.8 and 151.8 (both 4C, Tz C^5 + C^6), 156.6 (2C, Py $C^{2/6}$) 166.1 (2C, Tz C^3).

For $[Fe(L^6)_2][BF_4]_2$ (**1f**). Found: C, 43.0; H, 2.35; N, 18.2 %. Calcd. for $C_{26}H_{18}B_2F_8FeN_{10}O_2$: C, 42.7; H, 2.48; N, 19.1 %. ESMS *m/z* 279.0 $[Fe(L^6)_2]^{2+}$, 557.1 $[Fe(L^6)_2–H]^+$. ^{1}H NMR (CD_3NO_2) δ 7.43 (d, 3.1 Hz, 4H, Pyz H^5), 8.26 (d, 3.1 Hz, 4H, Pyz H^6), 8.57 (s, 4H, Py $H^{3/5}$), 9.48 (s, 4H, Pyz H^3). The

compound was too insoluble for a ^{13}C NMR spectrum to be recorded.

For $[Fe(L^7)_2][BF_4]_2$·½acetone (**1g**). This compound was recrystallised from acetone/diethyl ether. Found: C, 42.2; H, 2.90; N, 17.1 %. Calcd. for $C_{26}H_{18}B_2F_8FeN_{10}O_2$·½($C_3H_6O$): C, 43.4; H, 2.78; N, 18.4 %. ESMS *m/z* 252.1 $[HL^7]^+$, 279.0 $[Fe(L^7)_2]^{2+}$, 557.1 $[Fe(L^7)_2–H]^+$. ^1H NMR (CD_3NO_2) δ 7.24 (t, 4.9 Hz, 4H, Pym H^4), 8.00 (br s, 4H, s, 4H, Pym H^5), 8.76 (s, 4H, Py $H^{3/5}$), 8.83 (d, 4.2 Hz, 4H, Pym H^6). The compound was too insoluble for a ^{13}C NMR spectrum to be recorded.

For $[Co(L^1)_2][BF_4]_2$ (**2a**). Found: C, 47.2; H, 2.80; N, 15.8 %. Calcd. for $C_{28}H_{20}B_2CoF_8N_8$: C, 47.4; H, 2.84; N, 15.8 %. ESMS: *m/z* 263.6 $[Co(L^1)_2]^{2+}$, 614.2 $[Co(L^1)_2(BF_4)]^+$. ^1H NMR (CD_3NO_2): δ 10.2 (4H, Py H^4), 33.2 and 34.8 (both 4H, Py $H^{3/5}$ and Pyz H^5), 50.4 (4H, Pyz H^3), 91.3 (v br, 4H, Pyz H^6).

For $[Co(L^2)_2][BF_4]_2$ (**2b**). Found: C, 44.3; H, 2.40; N, 19.6 %. Calcd. for $C_{26}H_{18}B_2CoF_8N_{10}$: C, 44.4; H, 2.58; N, 19.9 %. ESMS: *m/z* 236.1 ($[HL^2]^+$), 264.6 $[Co(L^2)_2]^{2+}$. ^1H NMR (CD_3NO_2): δ 22.4 (2H, Py H^4), 32.8 (8H, Pyz H^5 and Py $H^{3/5}$), 45.7 (4H, Pyz H^3), 82.6 (v br, 4H, Pyz H^6).

For $[Co(L^3)_2][BF_4]_2$ (**2c**). Found: C, 38.8; H, 2.55; N, 22.4 %. Calcd. for $C_{24}H_{16}B_2CoF_8N_{12}$·$2H_2O$: C, 38.9; H, 2.72; N, 22.7 %. ESMS: *m/z* 265.5 $[Co(L^3)_2]^{2+}$, 314.0 $[Co(L^3)F]^+$, 550.1 $[Co(L^3)_2F]^+$, 618.1 $[Co(L^3)_2BF_4]^+$. ^1H NMR (CD_3NO_2): δ 24.2 (4H, central Pyz $H^{3/5}$), 33.1 (4H, distal Pyz H^5), 43.7 (4H, distal Pyz H^3), 81.5 (v br, 4H, distal Pyz H^6).

For $[Co(L^4)_2][BF_4]_2$ (**2d**). Found: C, 44.4; H, 2.60; N, 19.6 %. Calcd. for $C_{26}H_{18}B_2CoF_8N_{10}$: C, 44.4; H, 2.58; N, 19.9 %. ESMS: *m/z* 236.1 ($[HL^4]^+$), 258.1 $[Na(L^4)_2]^+$, 264.1 $[Co(L^4)_2]^{2+}$. ^1H NMR (CD_3NO_2): δ 11.2 (4H, Pym H^6), 23.6 (2H, Py H^4), 65.1 and 75.1 (both 4H, Py $H^{3/5}$ and Pym H^5), 70.0 (v br, 4H, Pym H^2).

For $[Co(L^5)_2][BF_4]_2$ (**2e**). Found: C, 35.5; H, 2.25; N, 25.9 %. Calcd. for $C_{22}H_{14}B_2F_8FeN_{14}$·$2H_2O$: C, 35.7; H, 2.45; N, 26.5 %. ESMS *m/z* 238.1 $[HL^5]^+$, 260.1 $[NaL^5]^+$, 497.1 $[Na(L^5)_2]^+$. ^1H NMR (CD_3NO_2) δ 9.1 (2H, Py H^4), 10.0 and 12.3 (both 4H, Py $H^{3/5}$ and Tz H^5), 19.1 (4H, Tz H^6).

For $[Co(L^6)_2][BF_4]_2$ (**2f**). Found: C, 40.8; H, 2.55; N, 18.2 %. Calcd. for $C_{26}H_{18}B_2CoF_8N_{10}O_2$·$2H_2O$: C, 40.5; H, 2.88; N, 18.2 %. ESMS: *m/z* 252.1 $[HL^6]^+$, 280.1 $[Co(L^6)_2]^{2+}$, 559.1 $[Co(L^6)_2–H]^+$. ^1H NMR (CD_3NO_2): δ 33.7 (4H, Pyz H^5), 59.7 and 64.8 (both 4H, Py $H^{3/5}$ and Pyz H^3), 97.3 (v br, 4H, Pyz H^6).

For $[Co(L^7)_2][BF_4]_2$·½acetone (**2g**). This compound was recrystallised from acetone/diethyl ether. Found: C, 43.1; H, 3.00; N, 17.9 %. Calcd. for $C_{26}H_{18}B_2CoF_8N_{10}O_2$·½($C_3H_6O$): C, 43.2; H, 2.77; N, 18.3 %. ESMS: *m/z* 280.5 $[Co(L^7)_2]^{2+}$, 560.1 $[Co(L^7)_2–H]^+$. ^1H NMR (CD_3NO_2): δ 9.6 (4H, Pym H^4), 25.7 (4H, Pym H^5), 83.2 (4H, Pym H^6). No peak assignable to Py $H^{3/5}$ was observed.

Single crystal *X*-ray structure determinations

All the single crystals in this work were grown by slow diffusion of diethyl ether vapour into nitromethane solutions of the compounds. Diffraction data were measured using a Bruker X8 Apex diffractometer fitted with an Oxford Cryostream low temperature device, using graphite-monochromated Mo-K_α radiation (λ = 0.71073 Å) generated by a rotating anode. Experimental details of the structure determinations in this study are given in Table 5. All the structures were solved by direct methods (*SHELXS97*[54]), and developed by full least-squares refinement on F^2 (*SHELXL97*[54]). Crystallographic figures were prepared using *X-SEED*,[55] which incorporates *POVRAY*.[56]

See http://dx.doi.org/10.1039/b000000x/ for crystallographic files in .cif format.

***X*-ray structure determination of $[Fe(L^1)_2][BF_4]_2$·$MeNO_2$ (1a·$MeNO_2$).** Crystals of this compound only showed significant diffraction below $2\theta = 50°$. The complex dication, two anions and solvent molecule all occupy general crystallographic positions. Both BF_4^- ions are disordered, each over two equally occupied sites labelled 'A' and 'B'. The refined restraints B–F = 1.38(2) and F...F = 2.25(2) Å were applied to these residues. The two O atoms of the nitromethane molecule were also disordered over two equally occupied orientations, which were modelled without restraints. Only the fully-occupied non-H atoms were refined

Table 5 Experimental details for the single crystal structure determinations in this study.

	1a·$MeNO_2$	**1d**·$3MeNO_2$	**2b**	**2d**
Molecular formula	$C_{29}H_{23}B_2F_8FeN_9O_2$	$C_{29}H_{27}B_2F_8FeN_{13}O_6$	$C_{26}H_{18}B_2CoF_8N_{10}$	$C_{26}H_{18}B_2CoF_8N_{10}$
M_r	759.03	883.11	703.05	703.05
Crystal class	monoclinic	monoclinic	tetragonal	monoclinic
Space group	$P2_1/c$	$P2_1/c$	$P\bar{4}2_1c$	$P2_1/c$
a (Å)	8.8102(4)	11.506(2)	8.7106(11)	18.672(4)
b (Å)	8.8297(4)	14.577(3)	–	10.146(2)
c (Å)	39.8492(18)	23.349(4)	19.178(2)	15.074(3)
β (°)	90.181(2)	96.533(9)	–	98.816(9)
V (Å^3)	3099.9(2)	3890.7(12)	1455.1(3)	2821.9(9)
Z	4	4	2	4
μ (Mo-K$_\alpha$) (mm^{-1})	0.581	0.485	0.679	0.700
T (K)	150(2)	150(2)	150(2)	150(2)
Measured reflections	64966	116433	29757	54457
Independent reflections	5504	11369	2176	8904
R_{int}	0.050	0.086	0.063	0.082
R_1, $I > 2\sigma(I)$[a]	0.072	0.073	0.061	0.048
wR_2, all data[b]	0.171	0.234	0.133	0.153
Goodness of fit	1.113	1.043	1.132	1.000
Flack parameter	–	–	0.48(4)	–

[a] $R = \Sigma[|F_o| - |F_c|] / \Sigma|F_o|$ [b] $wR = [\Sigma w(F_o^2 - F_c^2) / \Sigma wF_o^4]^{1/2}$

anisotropically, to maintain an observed data:parameter ratio of >10:1, while H atoms were placed in calculated positions and refined using a riding model. The highest residual Fourier peak of +1.4 $e.Å^{-3}$ lies within one of the disordered anions.

***X*-ray structure determination of $[Fe(L^4)_2][BF_4]_2 \cdot 3MeNO_2$ (1d·3MeNO$_2$).** The asymmetric unit contains one formula unit of the compound, with each residue lying on a general crystallographic position. One of the BF_4^- ions in the asymmetric unit, and two of the three nitromethane molecules, are disordered. The disordered anion was refined over two orientations, with refined occupancies of 0.56:0.44. The refined restraints B–F = 1.39(2) and F...F = 2.27(2) Å were applied to this residue. One disordered solvent molecule was modelled over two sites with refined occupancies of 0.69:0.31, while the other was refined over three orientations with fixed occupancies of 0.50, 0.25 and 0.25. The quarter-occupied sites in the latter residue shared a common half-occupied N atom. The disordered solvent was refined using the fixed restraints C–N = 1.45(2), N–O = 1.22(2), O...O = 2.09(2) and C...O = 2.30(2) Å. All non-H atoms with occupancy >0.5 were refined anisotropically, and all H atoms were placed in calculated positions and refined using a riding model. The highest residual Fourier peak of +1.2 $e.Å^{-3}$ is 0.8 Å from the iron atom.

***X*-ray structure determination of $[Co(L^2)_2][BF_4]_2$ (2b).** This structure was originally solved in *P*1, then transformed up to $P\bar{4}2_1c$ using the *ADSYMM* routine in *PLATON*.[57] The crystal was refined as a racemic twin. The asymmetric unit contains ¼ of a complex dication, with Co(1) occupying the crystallographic S_4 site [0, 0, 0] and N(2) and N(5) lying on the C_2 axis [0, 0, *z*]; and, half a BF_4^- anion spanning the C_2 axis [0, ½, *z*]. This half-anion was refined subject to the refined restraints B–F = 1.41(2) and F...F = 2.30(2) Å. All non-H atoms were refined anisotropically, and all H atoms were placed in calculated positions and refined using a riding model.

***X*-ray structure determination of $[Co(L^4)_2][BF_4]_2$ (2d)**. Each residue in this asymmetric unit lies on a general crystallographic site. One of the BF_4^- ions is disordered over two equally occupied orientations. This was modelled using the refined restraints B–F = 1.39(2) and F...F = 2.27(2) Å. All non-H atoms in the model were refined anisotropically, and H atoms were placed in calculated positions and refined using a riding model.

Other measurements

Elemental microanalyses were performed by the University of Leeds School of Chemistry microanalytical service. Infra-red spectra were obtained as nujol mulls pressed between NaCl windows between 600-4,000 cm^{-1}, using a Nicolet Avatar 360 spectrophotometer. Electrospray mass spectra (ES MS) were obtained on a Waters ZQ4000 spectrometer, from MeCN feed solutions. All mass peaks have the correct isotopic distributions for the proposed assignments. UV/vis/NIR spectra were run on a Perkin Elmer Lambda900 spectrophotometer using 1 cm quartz cells. *X*-band EPR spectra were obtained using a Bruker EMX spectrometer fitted with an ER4119HS resonator and ER4131VT cryostat. EPR spectra were simulated using Bruker *SimFonia*. X-ray powder diffraction measurements employed a Bruker D8 diffractometer, using Cu-K_α radiation. Samples were measured from $5 \leq 2\theta \leq 50^o$ in 0.0331° increments, using fixed slits. Powder pattern simulations were performed suing the *Lazy Pulverix* routine in *X-SEED*.[55]

Magnetic susceptibility measurements were performed on a Quantum Design SQUID magnetometer, in an applied field of 1000 G. A diamagnetic correction for the sample was estimated from Pascal's constants;[58] a diamagnetic correction for the sample holder was also applied to the data. The variable temperature data were also validated by comparison with room temperature magnetic moments, measured independently on a Sherwood Scientific susceptibility balance.

Electrochemical measurements were carried out using an Autolab PGSTAT20 voltammetric analyser, under an argon atmosphere, in predried CH_3CN containing 0.1 M $[^nBu_4N]BF_4$ as supporting electrolyte. Voltammetry experiments used a Pt disk working electrode, a Pt rod counter electrode and an Ag/AgCl reference electrode. All potentials quoted are referenced to an internal ferrocene/ferrocenium standard and were obtained at a scan rate (v) of 100 mV s^{-1}. The ferrocene/ferrocenium couple under these conditions was observed at $+0.38 \leq E_{½} \leq 0.42$ V *vs*. Ag/AgCl. Experiments involving the addition of base employed stoichiometric amounts of NBu_4OH (1.0 M solution in MeOH).

Acknowledgements

The authors thank Dr. Tim Comyn (School of Process, Environmental and Materials Engineering, University of Leeds) for assistance with the *X*-ray powder diffraction determinations. This work was funded by the EPSRC.

Notes and references

[a] *School of Chemistry, University of Leeds, Woodhouse Lane, Leeds LS2 9JT, U.K. Fax: (+44) 113 343 6565.Tel (+44) 113 343 6506. Email: M.A.Halcrow@leeds.ac.uk.*
[b] *School of Chemistry and Photon Science Institute, University of Manchester, Oxford Road, Manchester, UK M13 9PL.*

† Electronic Supplementary Information (ESI) available: additional magnetic susceptibility, UV/vis, EPR, powder diffraction and electrochemical data for the complexes in this study; and, crystallographic packing diagrams. CCDC reference numbers 893212-893215. For ESI and crystallographic data in CIF or other electronic format see DOI: 10.1039/###

‡ Dedicated to Professor David Cole-Hamilton on the occasion of his retirement and for his outstanding contribution to transition metal catalysis.

1 E. C. Constable, *Adv. Inorg. Chem. Radiochem.*, 1986, **30**, 69.
2 E. C. Constable, *Chem. Soc. Rev.*, 2007, **36**, 246.
3 I. Eryazici, C. N. Moorefield and G. R. Newkome, *Chem. Rev.*, 2008, **108**, 1834.
4 A. Wild, A. Winter, F. Schlütter and U. S. Schubert, *Chem. Soc. Rev.*, 2011, **40**, 1459.
5 U. S. Schubert, H. Hofmeier and G. S. Newkome, *Modern Terpyridine Chemistry*, Wiley-VCH, Weinheim, Germany, 2006, p. 229.
6 L. Flamigni, J.-P. Collin and J.-P. Sauvage, *Acc. Chem. Res.*, 2008, **41**, 857.

7 S. Hayami, Y. Komatsu, T. Shimizu, H. Kamihata and Y. H. Lee, *Coord. Chem. Rev.*, 2011, **255**, 1981.
8 R.-A. Fallahpour, *Synthesis*, 2003, 155; M. Heller and U. S. Schubert, *Eur. J. Org. Chem.*, 2003, 947.
9 H. Nishihara, K. Kanaizuka, Y. Nishimori and Y. Yamanoi, *Coord. Chem. Rev.*, 2007, **251**, 2674.
10 H. Hofmeier and U. S. Schubert, *Chem. Soc. Rev.*, 2004, **33**, 373.
11 E. C. Constable, *Coord. Chem. Rev.*, 2008, **252**, 842.
12 Y. Bodenthin, G. Schwarz, Z. Tomkowicz, M. Lommel, T. Geue, W. Haase, H. Möhwald, U. Pietsch and D. G. Kurth, *Coord. Chem. Rev.*, 2009, **253**, 2414; R. Shunmugam, G. J. Gabriel, K. A. Aamer and G. N. Tew, *Macromol. Rapid Commun.*, 2010, **31**, 784.
13 U. Ziener, E. Breuning, J.-M. Lehn, E. Wegelius, K. Rissanen, G. Baum, D. Fenske and G. Vaughan, *Chem. Eur. J.*, 2000, **6**, 4132.
14 E. A. Medlycott and G. S. Hanan, *Chem. Soc. Rev.*, 2005, **34**, 133.
15 S. Trumm, P. J. Panak, A. Geist and T. Fanghänel, *Eur. J. Inorg. Chem.*, 2010, 3022 and refs. therein.
16 See *e.g.* R. Liegghio, P. G. Potvin and A. B. P. Lever, *Inorg. Chem.*, 2001, **40**, 5485; M. I. J. Polson, E. A. Medlycott, G. S. Hanan, L. Mikelsons, N. J. Taylor, M. Watanabe, Y. Tanaka, F. Loiseau, R. Passalacqua and S. Campagna, *Chem. Eur. J.*, 2004, **10**, 3640; F. Nastasi, F. Loiseau, S. Campagna, E. A. Medlycott, M.-P. Santoni and G. S. Hanan, *Can. J. Chem.*, 2009, **87**, 254; J.-W. Dai, B.-Z. Li, Y.-L. Chen, G. Huang, B. Cai, Y. Yu and J.-Z. Wu, *Inorg. Chem. Commun.*, 2010, **13**, 625; J.-W. Dai, Z.-Y. Li, Y.-L. Chen, B. Cai, J.-Z. Wu, Y. Yu, *Z. Anorg. Allg. Chem.*, 2010, **636**, 2475.
17 M. Darabantu, L. Boully, A. Turck and N. Plé, *Tetrahedron*, 2005, **61**, 2897.
18 E. Bejan, H. A. Haddou, J. C. Daran and G. G. A. Balavoine, *Synthesis*, 1996, 1012.
19 J. Sauer, D. K. Heldmann and G. R. Pabst, *Eur. J. Org. Chem.*, 1999, 313.
20 M. A. Halcrow, *Coord. Chem. Rev.*, 2009, **253**, 2493.
21 M. A. Halcrow, *Chem. Soc. Rev.*, 2011, **40**, 4119.
22 P. Gütlich and H.A. Goodwin, (eds.), *Spin Crossover in Transition Metal Compounds I-III, Top. Curr. Chem.*, 2004, vols. **233-235**.
23 A. Bousseksou, G. Molnár, L. Salmon and W. Nicolazzi, *Chem. Soc. Rev.*, 2011, **40**, 3313.
24 H. A. Goodwin, *Top. Curr. Chem.*, 2004, **233**, 59.
25 M. Boča, R. F. Jameson and W. Linert, *Coord. Chem. Rev.*, 2011, **255**, 290.
26 C. A. Tovee, C. A. Kilner, J. A. Thomas and M. A. Halcrow, *CrystEngComm*, 2009, **11**, 2069.
27 M. A. Halcrow, *Chem. Commun.*, 2010, **46**, 4761.
28 G. Chastanet, C. A. Tovee, G. Hyett, M. A. Halcrow and J.-F. Létard, *Dalton Trans.*, 2012, **41**, 4896.
29 R. Docherty, F. Tuna, C. A. Kilner, E. J. L. McInnes and M. A. Halcrow, *Chem. Commun.*, 2012, **48**, 4055.
30 J. Groen, P. van Leeuwen and K. Vrieze, *J. Chem. Soc., Dalton Trans.*, 1998, 113.
31 E. C. Constable and M. D. Ward, *J. Chem. Soc., Dalton Trans.*, 1990, 1405.
32 M. L. Scudder, H. A. Goodwin and I. G. Dance, *New J. Chem.*, 1999, **23**, 695; J. McMurtrie and I. Dance, *CrystEngComm*, 2005, **7**, 216; J. McMurtrie and I. Dance, *CrystEngComm*, 2010, **12**, 2700.
33 C. A. Kilner and M. A. Halcrow, *Dalton Trans.*, 2010, **39**, 9008.
34 See *e.g.* A. T. Baker and H. A. Goodwin, *Aust. J. Chem.*, 1985, **38**, 207; P. Laine, A. Gourdon and J.-P. Launay, *Inorg. Chem.*, 1995, **34**, 5156; Y. Nakayama, Y. Baba, H. Yasuda, K. Kawakita and N. Ueyama, *Macromolecules*, 2003, **36**, 7953; M. K. Kabir, H. Tobita, H. Matsuo, K. Nagayoshi, K. Yamada, K. Adachi, Y. Sugiyama, S. Kitagawa and S. Kawata, *Cryst. Growth Des.*, 2003, **3**, 791; M. A. Tershansy, A. M. Goforth, L. Peterson jr., M. C. Burns, M. D. Smith and H. C. zur Loye, *Solid State Sci.*, 2007, **9**, 895.
35 M. A. Halcrow, *Chem. Soc. Rev.*, 2011, **40**, 4119.
36 The only high-spin $[Fe(terpy)_2]^{2+}$ derivatives are a small number of complexes bearing sterically bulky substitutents at the distal pyridyl groups. E. C. Constable, G. Baum, E. Bill, R. Dyson, R. van Eldik, D. Fenske, S. Kaderli, D. Morris, A. Neubrand, M. Neuburger, D. R. Smith, K. Wieghardt, M. Zehnder and A. D. Zuberbühler, *Chem. Eur. J.*, 1999, **5**, 498; S. Y. Brauchli, E. C. Constable, K. Harris, D. Häussinger, C. E. Housecroft, P. J. Rösel and J. A. Zampese, *Dalton Trans.*, 2010, **39**, 10739.
37 Some iron(II) complexes of 2,4-dipyridyl-6-aryl-1,3,5-triazine derivatives undergo gradual thermal spin-crossover. E. Medlycott, G. S. Hanan, T. S. M. Abedin and L. K. Thompson, *Polyhedron*, 2008, **27**, 493; S. K. Hain, F. W. Heinemann, K. Gieb, P. Müller, G. Hörner and A. Grohmann, *Eur. J. Inorg. Chem.*, 2010, 221.
38 A. Galet, A. B. Gaspar, M. C. Muñoz and J. A. Real, *Inorg. Chem.*, 2006, **45**, 4413.
39 R. Boča, *Coord. Chem. Rev.*, 2004, **248**, 757.
40 G. Agustí, C. Bartual, V. Martínez, F. J. Muñoz-Lara, A. B. Gaspar, M. C. Muñoz and J. A. Real, *New J. Chem.*, 2009, **33**, 1262; G. Juhász, R. Matsuda, S. Kanegawa, K. Inoue, O. Sato and K. Yoshizawa, *J. Am. Chem. Soc.*, 2009, **131**, 4560.
41 J. G. Schmidt, W. S. Brey jr. and R. C. Stoufer, *Inorg. Chem.*, 1967, **6**, 268; S. Kremer, W. Henke and D. Reinen, *Inorg. Chem.*, 1982, **21**, 3013; P. Nielsen, H. Toftlund, A. D. Bond, J. F. Boas, J. R. Pilbrow, G. R. Hanson, C. Noble, M. J. Riley, S. M. Neville, B. Moubaraki and K. S. Murray, *Inorg. Chem.*, 2009, **48**, 7033.
42 J. S. Judge and W. A. Baker jr., *Inorg. Chim. Acta*, 1967, **1**, 68; B. N. Figgis, E. S. Kucharski and A. H. White, *Aust. J. Chem.*, 1983, **36**, 1537.
43 P. S. Braterman, J.-I. Song and R. D. Peacock, *Inorg. Chem.*, 1992, **31**, 555; T. G. Spence, B. T. Trotter and L. A. Posey, *J. Phys. Chem. A*, 1998, **102**, 7779.
44 J. Chambers, B. Eaves, D. Parker, R. Claxton, P. S. Ray and S. J. Slattery, *Inorg. Chim. Acta*, 2006, **359**, 2400.
45 M. Sjödin, J. Gätjens, L. C. Tabares, P. Thuéry, V. L. Pecoraro and S. Un, *Inorg. Chem.*, 2008, **47**, 2897.
46 J. England, C. C. Scarborough, T. Weyhermüller, S. Sproules and K. Wieghardt, *Eur. J. Inorg. Chem.*, 2012, 4605.
47 C. Arana, S. Yan, M. Keshavarz-K, K. T. Potts and H. D. Abruña, *Inorg. Chem.*, 1992, **31**, 3680.
48 M. G. B. Drew, M. R. St. J. Foreman, A. Geist, M. J. Hudson, F. Marken, V. Norman and M. Weigl, *Polyhedron*, 2006, **25**, 888.
49 A. B. P. Lever, in: *Comprehensive Coordination Chemistry II – from Biology to Nanotechnology*, eds. J. McCleverty and T. J. Meyer, Elsevier, Oxford, 2003; vol. 2 (ed. A. B. P. Lever), ch. 2.19, p. 251.
50 A. B. P. Lever, *Inorg. Chem.*, 1990, **29**, 1271.
51 T. Brinck, J. S. Murray, P. Politzer and R. E. Carter, *J. Org. Chem.*, 1991, **56**, 2934; R. Casasnovas, J. Frau, J. Ortega-Castro, A. Salvà, J. Donoso and F. Muñoz, *J. Mol. Struct. THEOCHEM*, 2009, **912**, 5.
52 R. J. Smithson, C. A. Kilner, A. R. Brough and M. A. Halcrow, *Polyhedron*, 2003, **22**, 725; R. Mohammed, G. Chastanet, F. Tuna, T. L. Malkin, S. A. Barrett, C. A. Kilner, J.-F. Létard and M. A. Halcrow, *Eur. J. Inorg. Chem.*, in the press (doi: 10.1002/ejic.201201100).
53 E. C. Constable and A. M. W. Cargill Thompson, *J. Chem. Soc., Dalton Trans.*, 1992, 2947; J. McMurtrie and I. Dance, *CrystEngComm*, 2005, **7**, 230.
54 G. M. Sheldrick, *Acta Crystallogr., Sect. A*, 2008, **64**, 112
55 L. J. Barbour, *J. Supramol. Chem.*, 2001, **1**, 189.
56 *POVRAY*, v. 3.5, Persistence of Vision Raytracer Pty. Ltd., Williamstown, Victoria, Australia, 2002. http://www.povray.org.
57 A. L. Spek, *J. Appl. Cryst.*, 2003, **36**, 7.
58 C. J. O'Connor, *Prog. Inorg. Chem.*, 1982, **29**, 203.

Iron(II) and Cobalt(II) Complexes of Tris-Azinyl Analogues of 2,2':6',2''-Terpyridine

Laurence J. Kershaw Cook,[a] Floriana Tuna,[b] and Malcolm A. Halcrow[a,*]

[a]*School of Chemistry, University of Leeds, Woodhouse Lane, Leeds LS2 9JT, U.K..*
[b]*School of Chemistry, University of Manchester, Oxford Road, Manchester M13 9PL, UK*
Email: M.A.Halcrow@leeds.ac.uk

Supporting Information

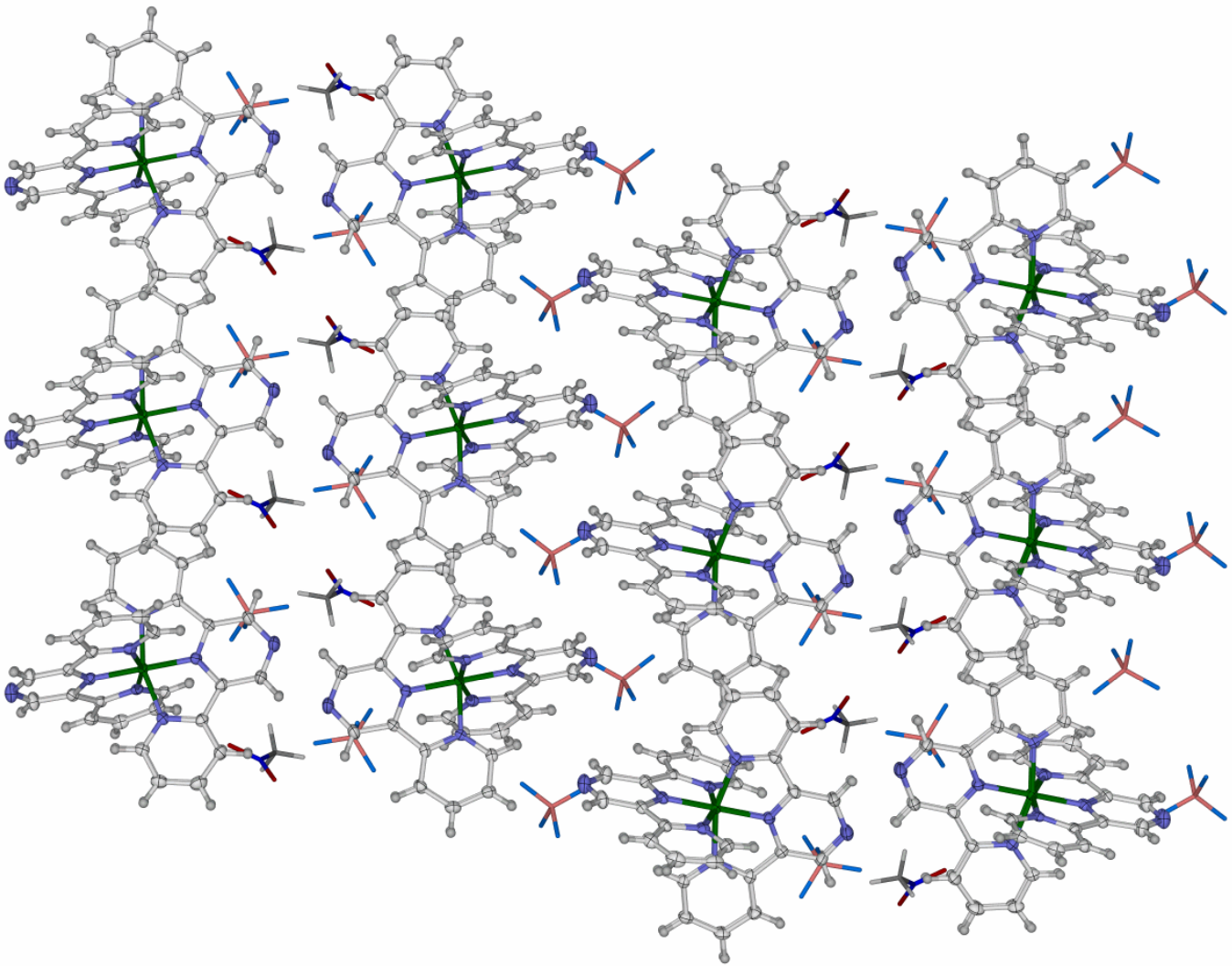

Figure S1. Partial packing diagram for **1a**·$MeNO_2$. The view is perpendicular to the (100) crystal plane, and only one orientation of the disordered anion and solvent residues is shown. Displacement ellipsoids are at the 50 % probability level except for the BF_4^- ions and nirtomethane molecules, which have been de-emphasised for clarity. Colour code: C, white; H, grey; B, pink; F, cyan; Fe, green; N, blue; O, red.

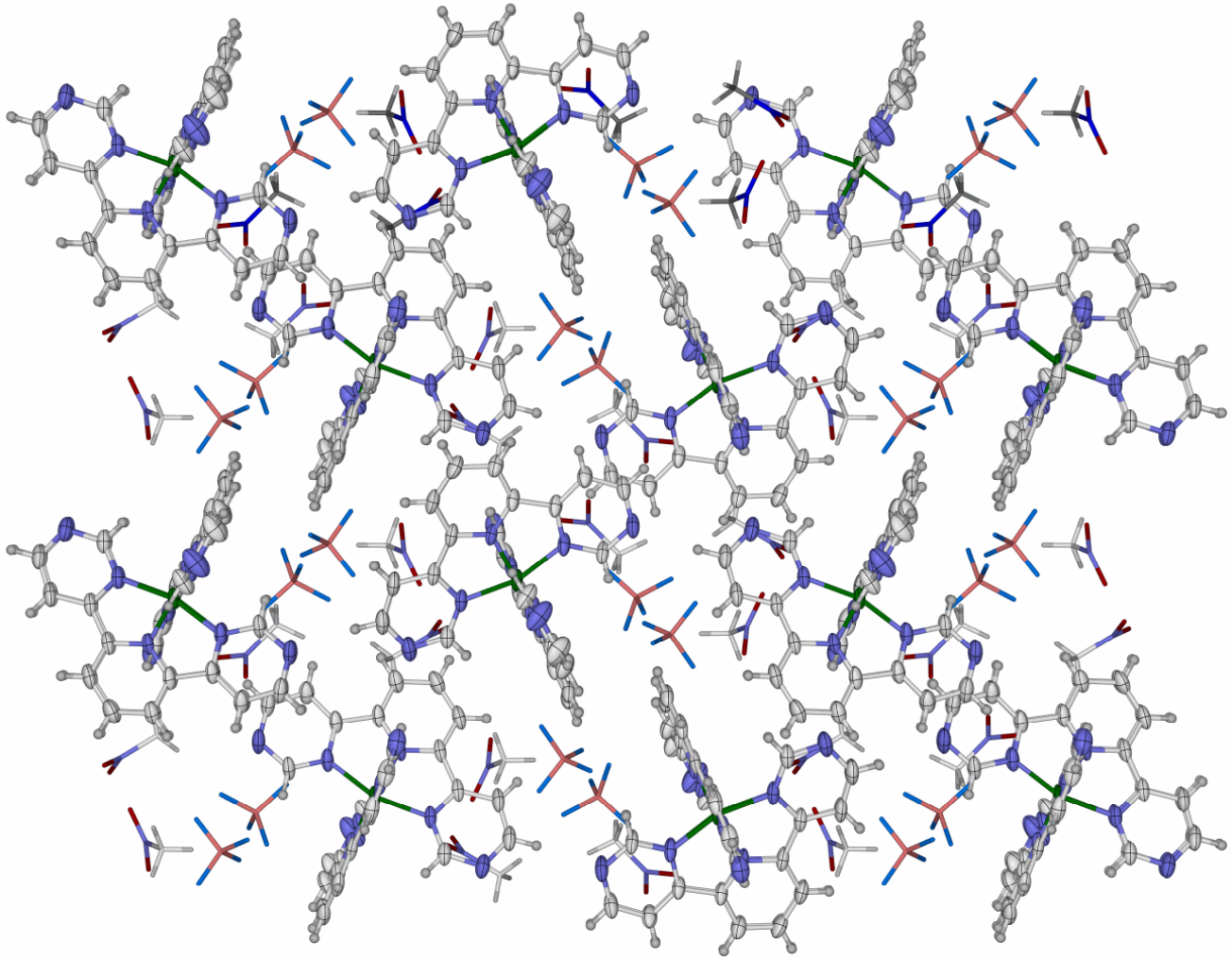

Figure S2. Partial packing diagram for **1d**·3MeNO$_2$. The view is perpendicular to the (100) crystal plane, and only one orientation of the disordered anion and solvent residues is shown. Displacement ellipsoids are at the 50 % probability level except for the BF_4^- ions and nirtomethane molecules, which have been de-emphasised for clarity. Colour code: C, white; H, grey; B, pink; F, cyan; Fe, green; N, blue; O, red.

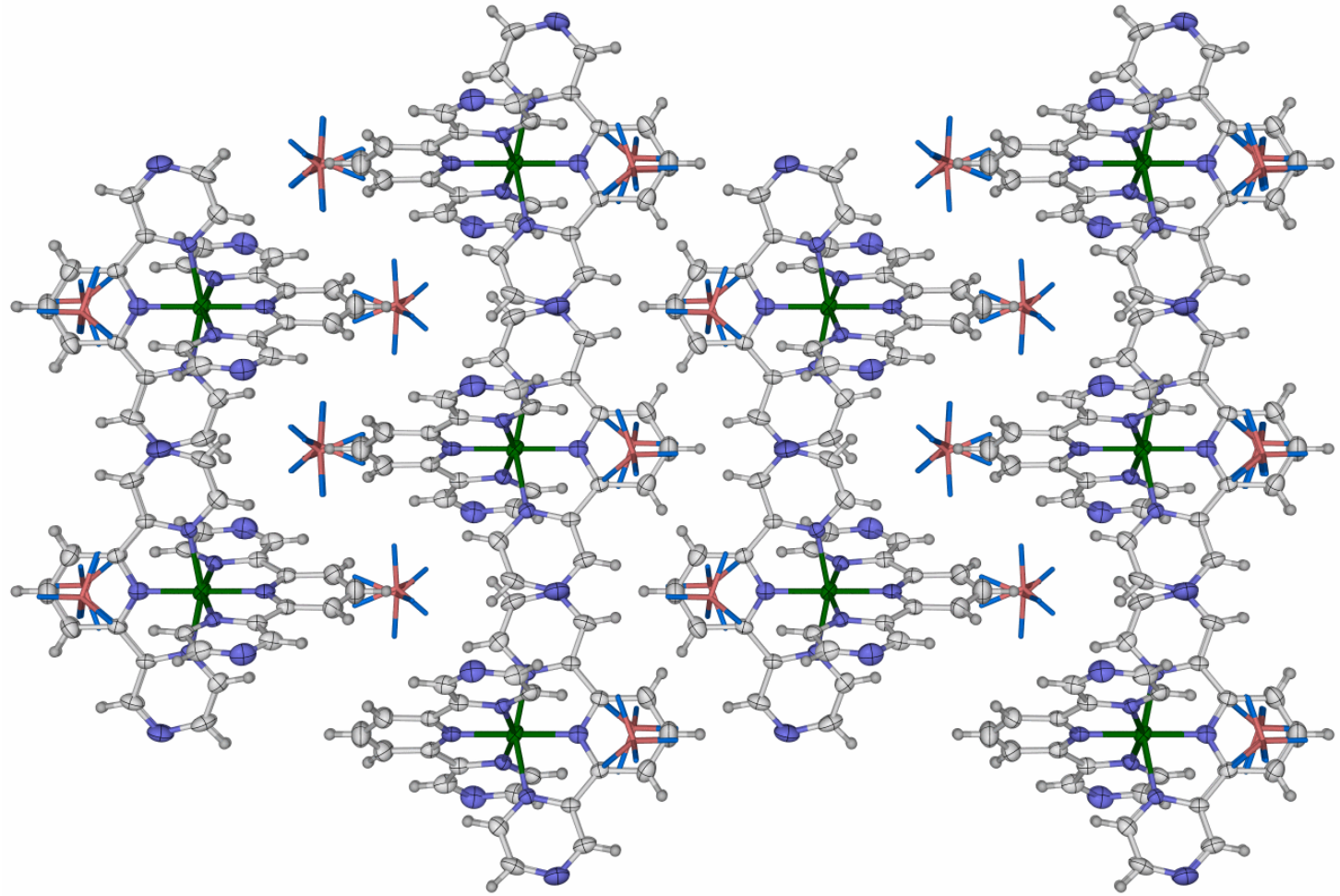

Figure S3. Partial packing diagram for **2b**. The view is perpendicular to the (100) crystal plane, and only one of the two BF_4^- environments in each anion site is shown. Displacement ellipsoids are at the 50 % probability level except for the BF_4^- ions which have been de-emphasised for clarity. Colour code: C, white; H, grey; B, pink; Co, green; F, cyan; N, blue.

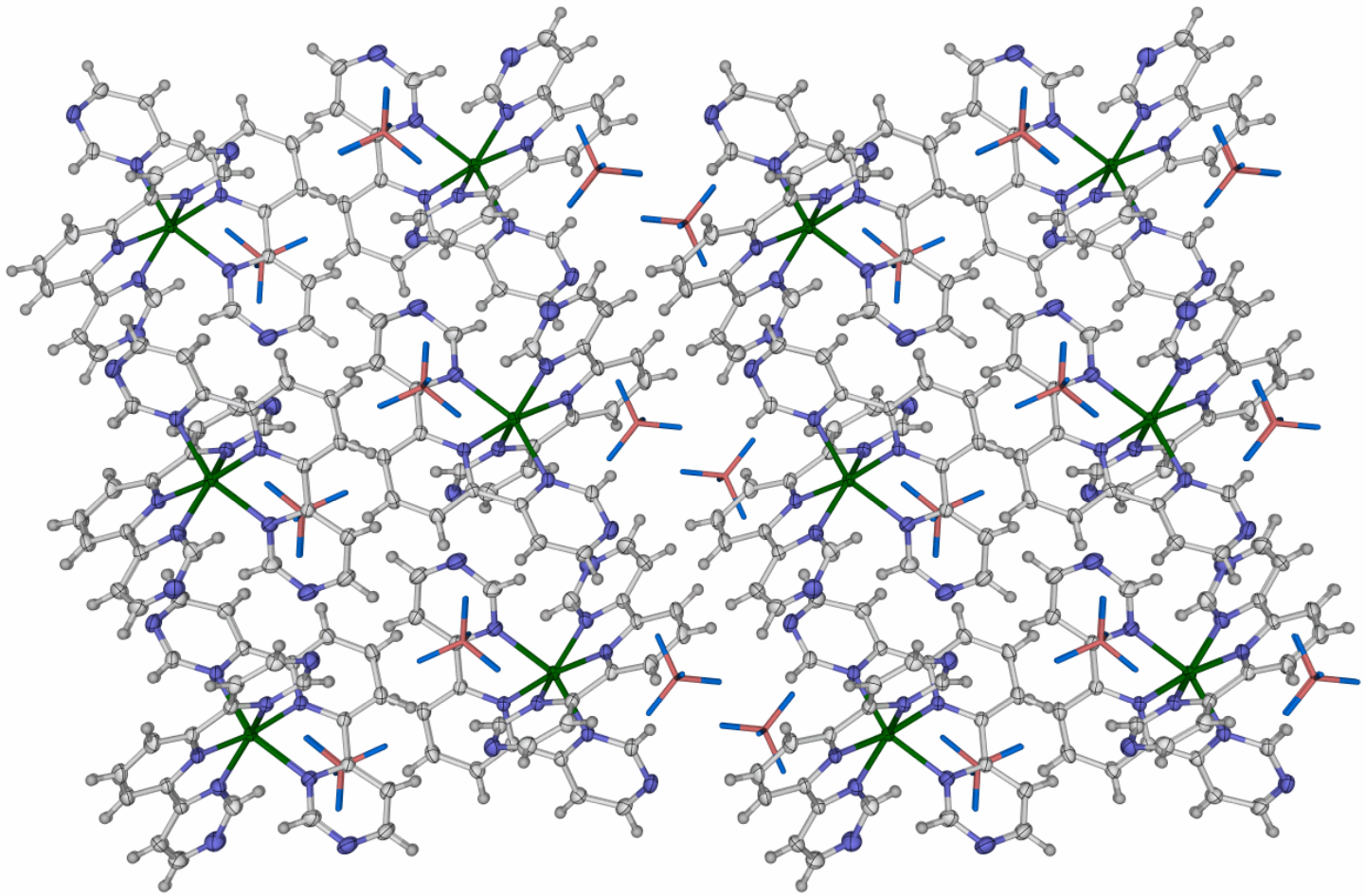

Figure S4. Partial packing diagram for **2d**. The view is perpendicular to the (010) crystal plane, and only one orientation of the disordered anion is shown. Displacement ellipsoids are at the 50 % probability level except for the BF_4^- ions which have been de-emphasised for clarity. Colour code: C, white; H, grey; B, pink; Co, green; F, cyan; N, blue.

Table S1. Metric parameters for intermolecular π-π interactions in crystal structures in this work (Å, °). Symmetry codes: (i) *x*, *y*, *z*; (ii) *x*, –1+*y*, *z*; (iii) –*x*, 1–*y*, *z*.

	Dihedral angle	Interplanar spacing	Horizontal offset
1a·$MeNO_2$			
[C(8)-C(13)]...[C(14^{i})-C(19^{i})]	7.1(2)	3.345(15)	1.80
[C(26)-C(31)]...[C(32^{ii})-C(37^{ii})]	1.95(18)	3.452(16)	2.07
2b			
[C(6)-C(11)]…[C(6^{iii})-C(11^{iii})]	1.01(14)	3.567(14)	1.18

There are no intermolecular π-π interactions in the structures of **1d**·3$MeNO_2$ and **2d**.

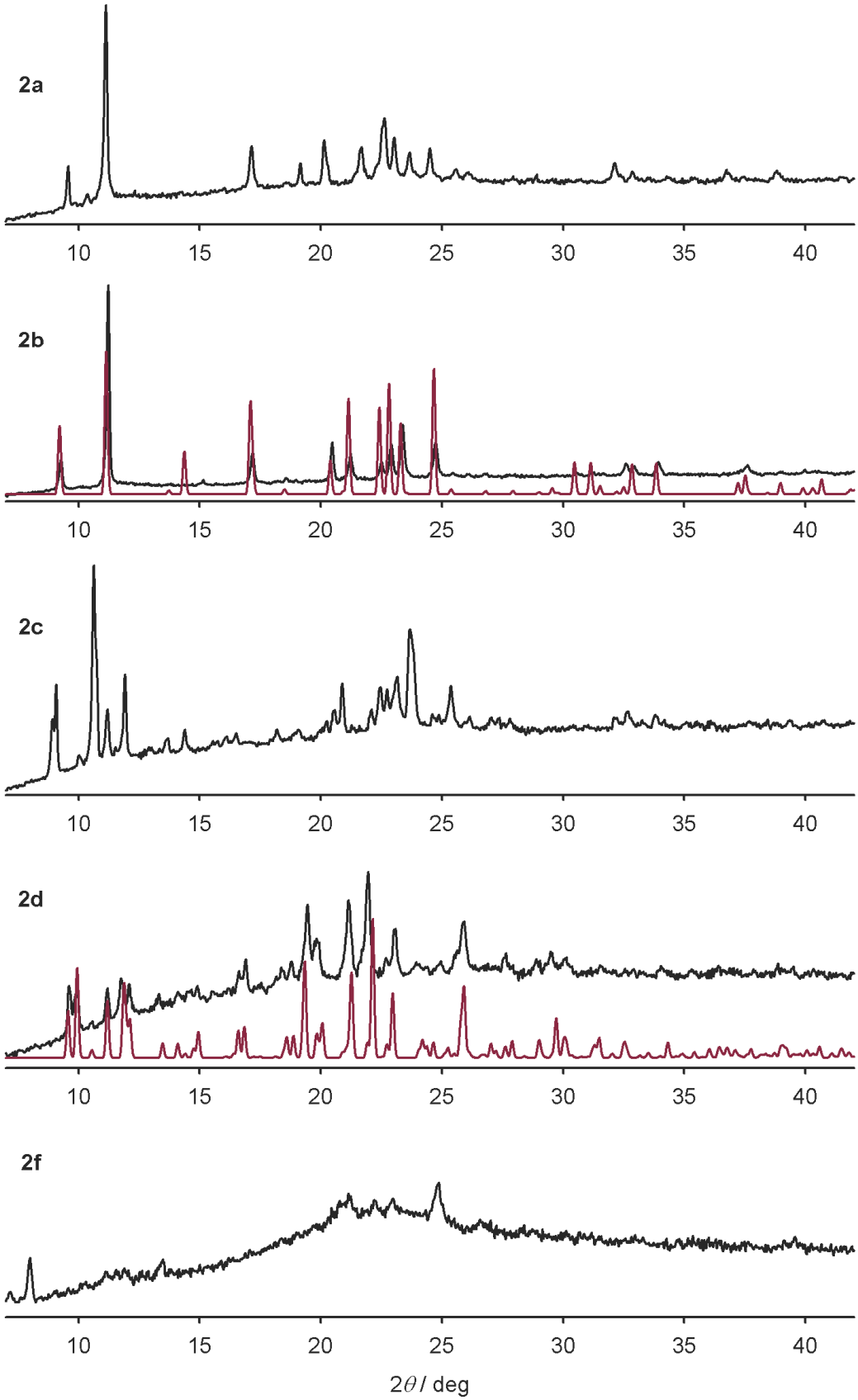

Figure S5. Selected *X*-ray powder diffraction data from cobalt complexes in this work. Simulations based on the single crystal *X*-ray structures of **2b** and **2d** are shown in red.

Table S2. *X*-band powder EPR parameters for the cobalt compounds in this work (Figs. S1 and S2). The quoted *g* and *A* values are the results of simulations, and hyperfine couplings are to ^{59}Co ($I = 7/2$). iso = isotropic; br = broad; w = weak.

	120±5 K	180 K	290 K
$[Co(terpy)_2][BF_4]_2$[4]	axial; $g_{\parallel} = 2.22$, $g_{\perp} = 2.12$	iso; $g = 2.12$	–[a]
$[Co(terpyOH)_2][BF_4]_2$	iso; $g = 2.11$	iso; $g = 2.12$	–[a]
$[Co(L^1)_2][BF_4]_2$ (**2a**)	axial; $g_{\parallel} = 2.22$[b], $g_{\perp} = 2.12$	iso; $g = 2.12$	–[a]
$[Co(L^2)_2][BF_4]_2$ (**2b**)	iso; $g = 2.11$	iso; $g = 2.12$	br w iso; $g = 2.14$
$[Co(L^3)_2][BF_4]_2$ (**2c**)	iso; $g = 2.11$	iso; $g = 2.11$[b]	iso; $g = 2.15$
$[Co(L^4)_2][BF_4]_2$ (**2d**)	axial; $g_{\parallel} = 2.23$, $A_{\parallel} = 98$ G, $g_{\perp} = 2.13$	axial; $g_{\parallel} = 2.20$, $A_{\parallel} = 88$ G, $g_{\perp} = 2.13$	w axial; $g_{\parallel} = 2.18$, $A_{\parallel} = 87$ G, $g_{\perp} = 2.13$
$[Co(L^5)_2][BF_4]_2$ (**2e**)	iso; $g = 2.12$[b]	iso; $g = 2.12$[b]	w iso; $g = 2.11$[b]
$[Co(L^5)_2][BF_4]_2$ (**2f**)	iso; $g = 2.12$	iso; $g = 2.12$	br w iso; $g = 2.14$
$[Co(L^6)_2][BF_4]_2$ (**2g**)	axial; $g_{\parallel} = 2.23$, $A_{\parallel} = 100$ G, $g_{\perp} = 2.12$	br iso; $g = 2.12$[b]	–[a]

[a]EPR-silent. [b]Some evidence for hyperfine coupling is apparent in the parallel region of this spectrum, but the lines were too broad to simulate accurately.

The best resolved low-temprature spectra are shown by **2d** and **2g**, which also have the smallest low-spin populations at 120 K (Table S1). Thus, those two samples have the most magnetically dilute $S = 1/2$ cobalt centres, at a temperature where dipolar relaxation by the remainder $S = 3/2$ cobalt sites is weak.

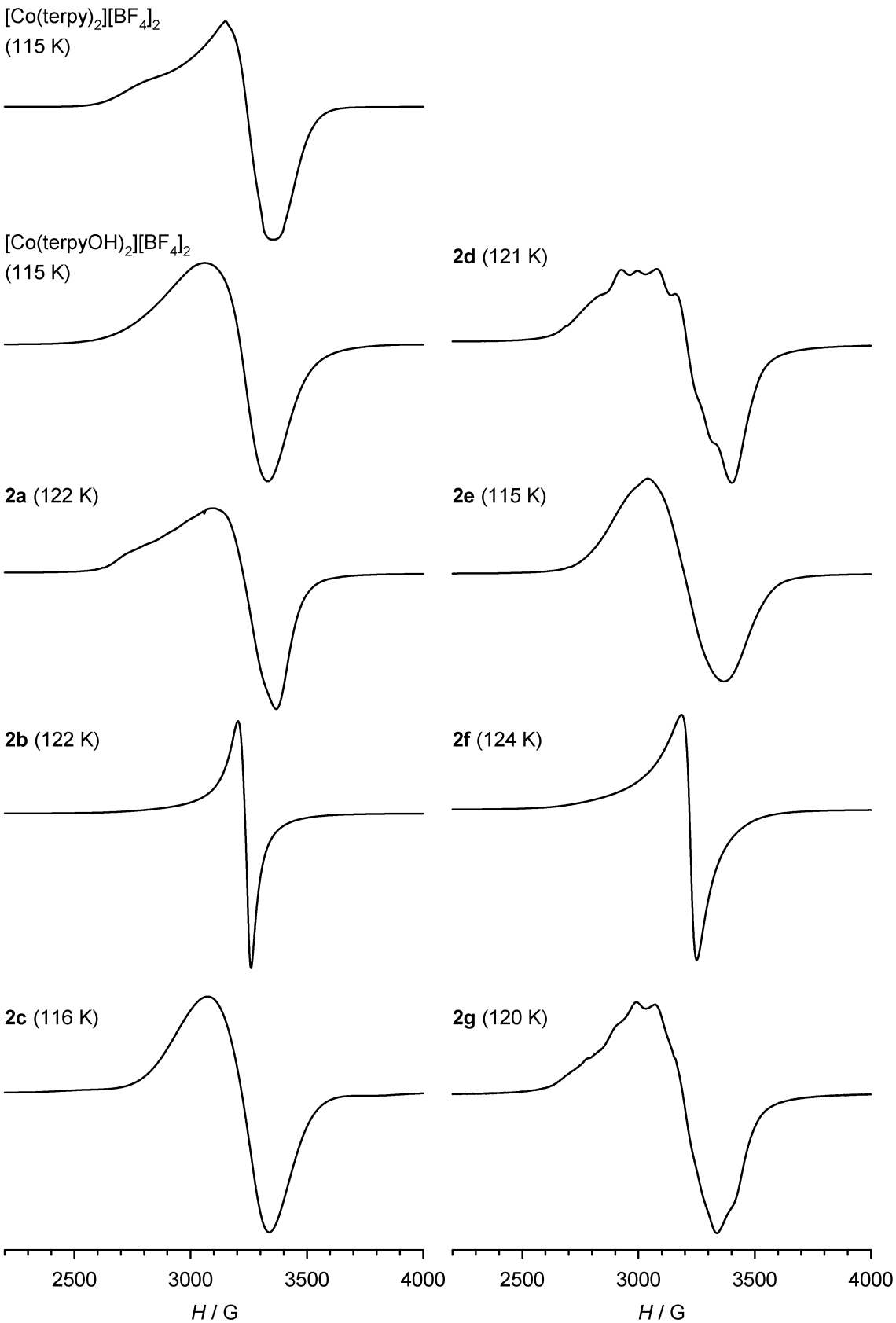

Figure S6. Powder *X*-band EPR spectra of the cobalt(II) complexes in this work, at around 120 K. The spectrum of $[Co(terpy)_2][BF_4]_2$ is taken from ref. [4].

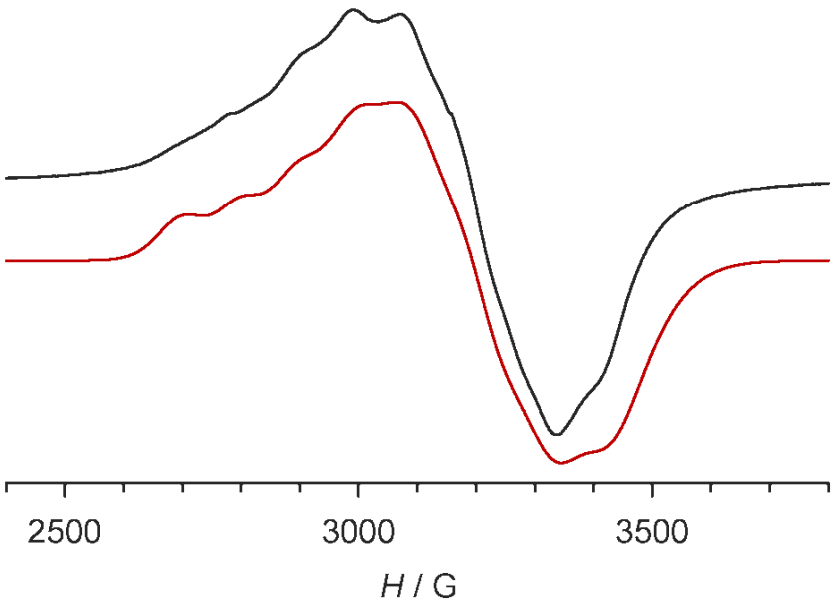

Figure S7. Experimental (black) and simulated (red) *X*-band powder EPR spectrum of **2g** at 120 K. Simulation parameters: $g_{\parallel} = 2.23$, $g_{\perp} = 2.13$, $A_{\parallel}\{^{59}\mathrm{Co}\} = 100$ G.

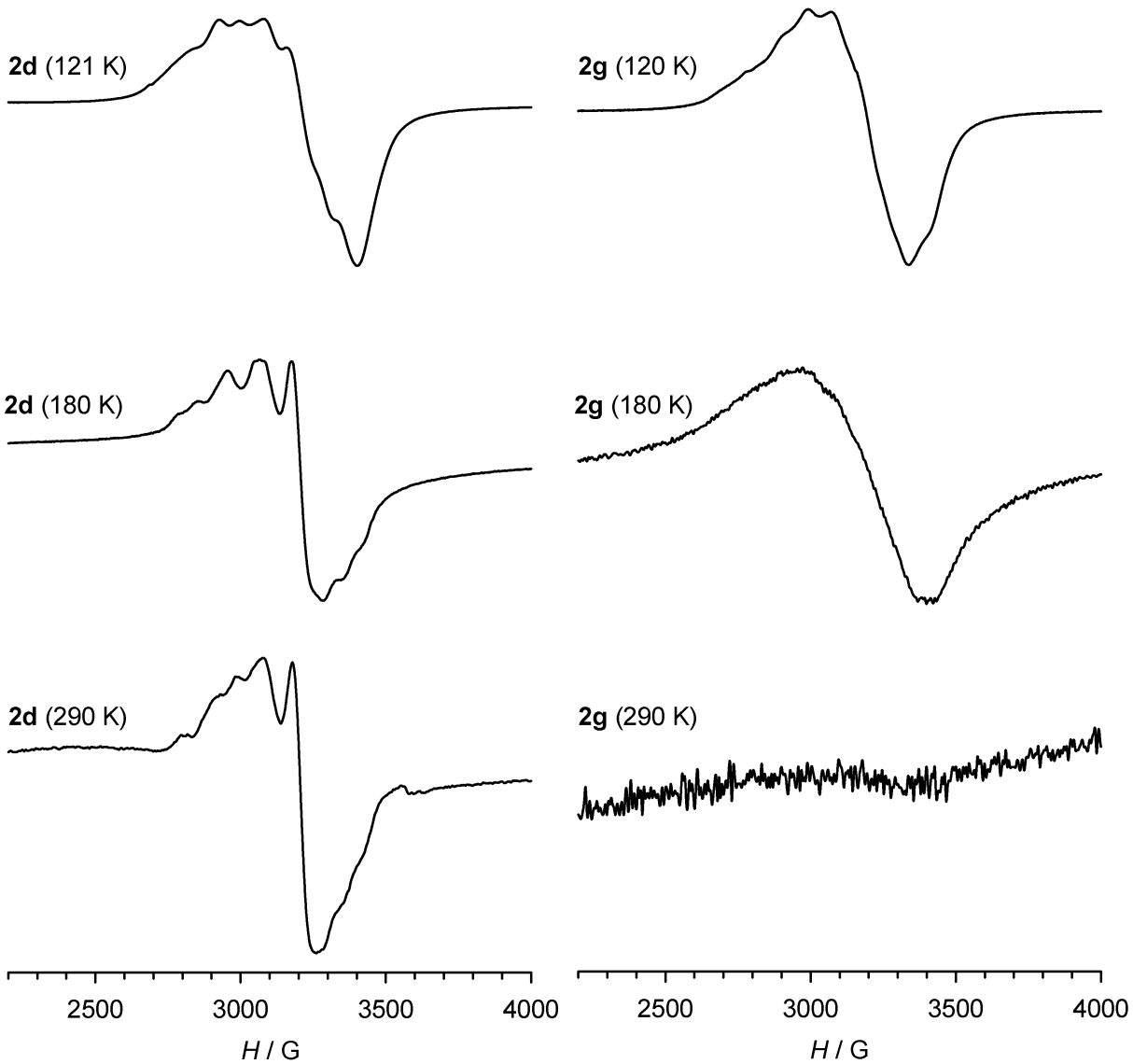

Figure S8. Variable temperature powder *X*-band EPR data for **2d** and **2g**.

The narrow linewidth and high resolution of the spectrum of **2d** at 290 K contrasts with most of the other compounds in this work. A similar lack of line-broadening is also shown by **2c** at higher temperatures, although its spectrum is not so well resolved (Fig. S1). Solid **2c** and **2d** are predominantly low-spin, and high-spin, respectively at room temperature (Table S1, and Fig. 3 of the main paper).

The behaviour of **2g** at higher temperatures is typical of the other seven complexes studied.

Table S3 UV/vis data for the complexes in this work (MeCN, 298 K). Spectra for **1e** and **2e** were not measured, because of the difficulty in obtaining pure samples of those compounds. The data for $[M(terpy)_2][BF_4]_2$ (M^{2+} = Fe^{2+} and Co^{2+}) closely resemble the spectra reported for salts of those compounds in other solvents.[5,6]

	λ_{max}, nm (ε_{max}, 10^3 dm^3 mol^{-1} cm^{-1})
$[Fe(terpy)_2][BF_4]_2$	220 (sh), 273 (41.6), 280 (37.5), 319 (51.1), 504 (sh), 552 (11.1), 590 (sh)
$[Fe(terpyOH)_2][BF_4]_2$	243 (54.5), 272 (52.0), 281 (sh), 315 (45.0), 362 (5.1), 515 (sh), 553 (11.6)
1a	249 (sh), 278 (28.8), 328 (31.3), 345 (sh), 552 (7.9), 590 (sh)
1b	230 (36.4), 246 (sh), 285 (34.9), 330 (18.2), 350 (sh), 552 (3.1), 590 (sh)
1c	221 (36.5), 227 (sh), 243 (30.9), 282 (47.1), 339 (34.0), 360 (23.5), 462 (1.8), 545 (7.9), 580 (sh)
1d	220 (34.8), 263 (sh), 272 (26.1), 278 (sh), 315 (32.9), 319 (sh), 574 (5.7), 610 (sh)
1f	218 (21.6), 238 (24.9), 245 (sh), 283 (28.3), 323 (sh), 355 (sh), 483 (sh), 586 (2.7), 655 (sh)
1g	252 (54.6), 292 (sh), 305 (10.8), 397 (4.8), 545 (6.1)
$[Co(terpy)_2][BF_4]_2$	225 (sh), 273 (30.2), 280 (31.1), 317 (33.8), 506 (1.0), 551 (sh)
$[Co(terpyOH)_2][BF_4]_2$	228 (58.4), 275 (34.8), 303 (sh), 379 (7.2), 454 (0.7)
2a	280 (24.2), 337 (21.2), 348 (sh), 509 (1.1)
2b	288 (52.7), 332 (31.8), 511 (1.1)
2c	225 (33.5), 285 (41.4), 346 (19.6), 474 (sh), 510 (0.8), 558 (sh)
2d	263 (sh), 280 (sh), 315 (44.6), 521 (0.4)
2f	232 (27.8), 285 (18.0), 312 (sh), 386 (3.8), 499 (1.0)
2g	232 (40.6), 251 (52.7), 379 (4.7), 480 (0.8)

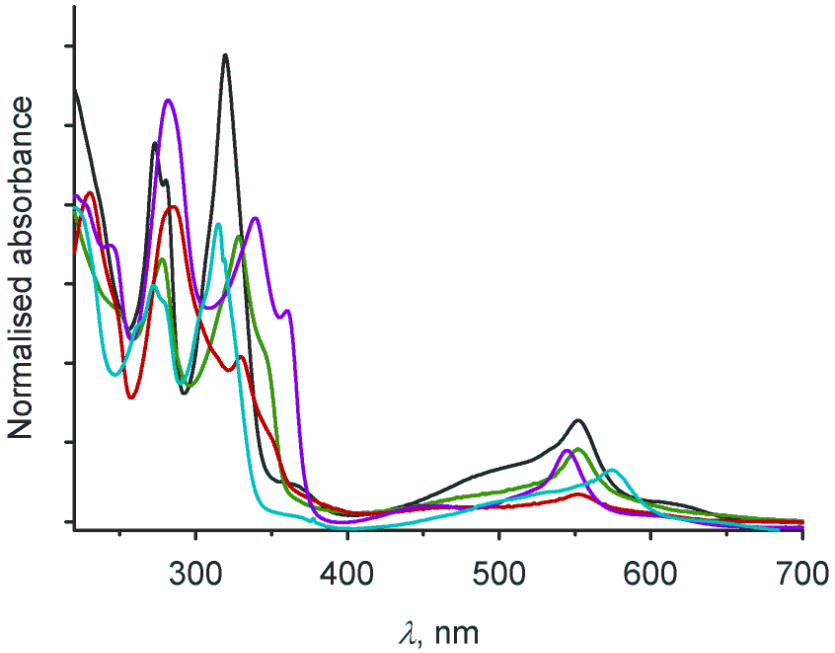

Figure S9. UV/vis spectra (MeCN, 298 K) of $[Fe(terpy)_2][BF_4]_2$ (black), **1a** (green), **1b** (red), **1c** (purple) and **1d** (cyan). These data are tabulated in the main paper.

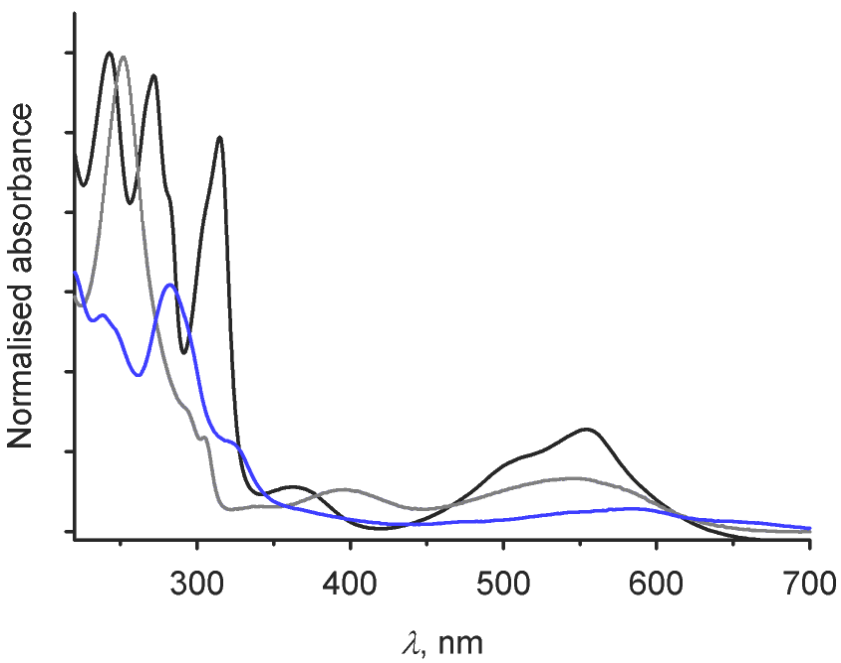

Figure S10. UV/vis spectra (MeCN, 298 K) of $[Fe(terpyOH)_2][BF_4]_2$ (black), **1f** (blue) and **1g** (grey). These data are tabulated in the main paper.

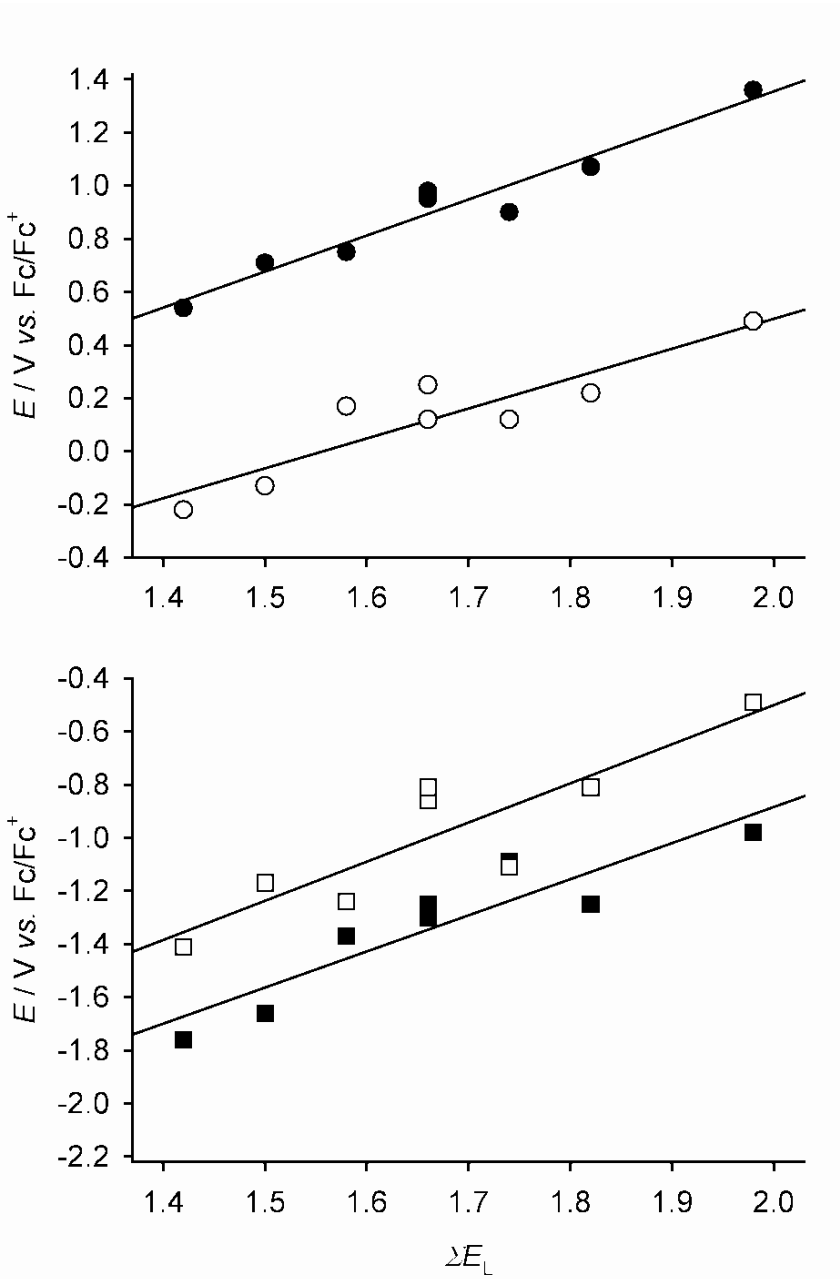

Figure S11. Correlations between $E_{½}$ and ΣE_L[7] for the oxidation (top) and first reduction (bottom) processes shown by the complexes: (●) iron oxidation; (○) cobalt oxidation; (■) iron reduction; (□) cobalt reduction. Ep$_a$ or Ep$_c$ peak potentials are plotted for irreversible processes, but this has only a small effect on the scatter in the graphs. These data are listed in Table 3 of the main article.

The E_L value for 4-hydroxypyridine employed in this analysis (0.21) is an estimated one, based on the published value of 4-(dimethylamino)pyridine (E_L = –0.19[8]) and the σ_p Hammett parameters for dimethylamino and hydroxy substituents, which are known to correlate with $E_{½}$ in $[M(terpy)_2]^{2+}$ derivatives (M^{2+} = Fe^{2+}, Co^{2+} and Ru^{2+}).[9] The complexes **1e** and **2e** are omitted from these graphs, because no E_L value for 1,2,4-triazine is available.

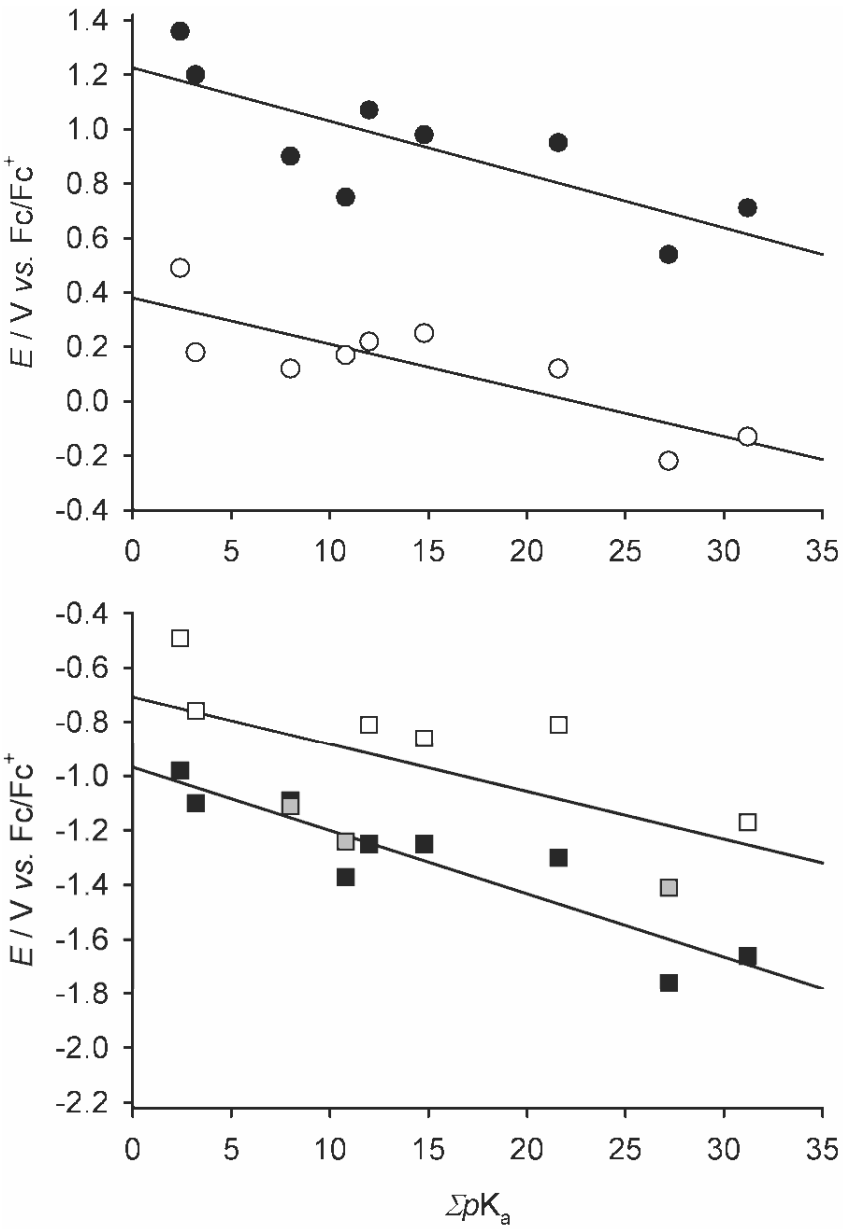

Figure S12. Correlations between $E_{½}$ and ΣpK_a for the oxidation (top) and first reduction (bottom) processes shown by the complexes: (●) iron oxidation; (○) cobalt oxidation; (■) iron reduction; (□ and ■) cobalt reduction. Ep_a or Ep_c peak potentials are plotted for irreversible processes, but this has only a small effect on the scatter in the graphs. These data are listed in Table 3 of the main article.

The graphs are plotted to the same vertical scale as in Fig. S6, to aid comparison.

There is more scatter on the cobalt reduction plot than for the other processes in the Figure. The grey data points are the cobalt complexes of the hydroxylated ligands terpyOH, L^6 and L^7 which all show lower than expected *E* values compared to the other complexes in that series. That tentatively supports the suggestion in the main article that, among the cobalt reductions, the white data points are metal-based reductions while the grey data points may be ligand-based.

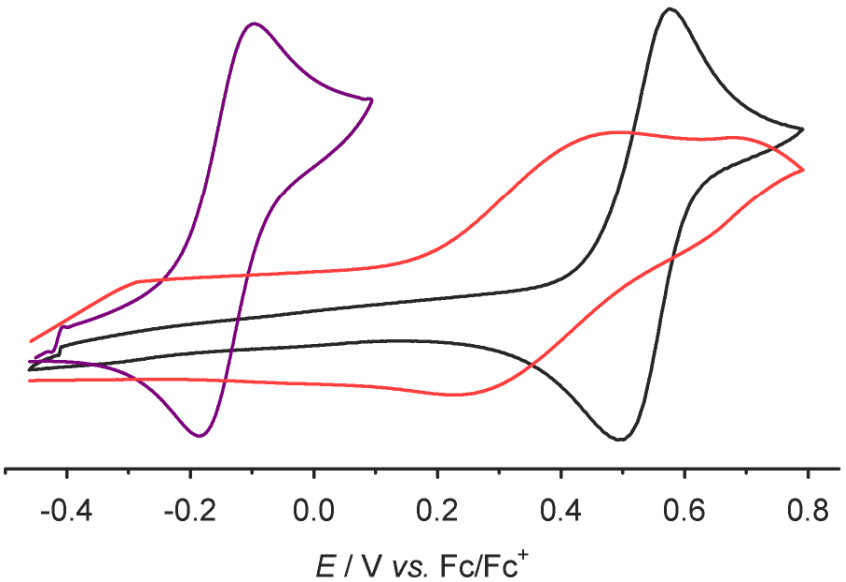

Figure S13. The Fe(III)/(II) couple in the cyclic voltammograms of the same solution of $[Fe(terpyOH)_2][BF_4]_2$ in the presence of 0 (black), 1 (red) and 2 (purple) equiv NBu_4OH (MeCN/0.1 M NBu_4BF_4, 298 K). These data are listed in Table 4 of the main article.

References

[1] G. Agustí, C. Bartual, V. Martínez, F. J. Muñoz-Lara, A. B. Gaspar, M. C. Muñoz and J. A. Real, *New J. Chem.*, 2009, **33**, 1262.

[2] C. J. O'Connor, *Prog. Inorg. Chem.*, 1982, **29**, 203.

[3] R. Boča, *Coord. Chem. Rev.*, 2004, **248**, 757.

[4] C. A. Kilner and M. A. Halcrow, *Dalton Trans.*, 2010, **39**, 9008.

[5] P. S. Braterman, J.-I. Song and R. D. Peacock, *Inorg. Chem.*, 1992, **31**, 555; T. G. Spence, B. T. Trotter and L. A. Posey, *J. Phys. Chem. A*, 1998, **102**, 7779.

[6] S. Kremer, W. Henke and D. Reinen, *Inorg. Chem.*, 1982, **21**, 3013.

[7] A. B. P. Lever, *Inorg. Chem.*, 1990, **29**, 1271.

[8] A. J. L. Pombeiro, *J. Organomet. Chem.*, 2005, **690**, 6021.

[9] M. Maestri, N. Armaroli, V. Balzani, E. C. Constable and A. M. W. Cargill Thompson, *Inorg. Chem.*, 1995, **34**, 2159; J. Chambers, B. Eaves, D. Parker, R. Claxton, P. S. Ray and S. J. Slattery, *Inorg. Chim. Acta*, 2006, **359**, 2400.